

A Master Equation Formalism for Macroscopic Modeling of Asynchronous Irregular Activity States

Sami El Boustani

elbousta@unic.cnrs-gif.fr

Alain Destexhe

destexhe@iaf.cnrs-gif.fr

*Unité de Neurosciences Intégratives et Computationnelles, CNRS,
91198 Gif-sur-Yvette, France*

Many efforts have been devoted to modeling asynchronous irregular (AI) activity states, which resemble the complex activity states seen in the cerebral cortex of awake animals. Most of models have considered balanced networks of excitatory and inhibitory spiking neurons in which AI states are sustained through recurrent sparse connectivity, with or without external input. In this letter we propose a mesoscopic description of such AI states. Using master equation formalism, we derive a second-order mean-field set of ordinary differential equations describing the temporal evolution of randomly connected balanced networks. This formalism takes into account finite size effects and is applicable to any neuron model as long as its transfer function can be characterized. We compare the predictions of this approach with numerical simulations for different network configurations and parameter spaces. Considering the randomly connected network as a unit, this approach could be used to build large-scale networks of such connected units, with an aim to model activity states constrained by macroscopic measurements, such as voltage-sensitive dye imaging.

1 Introduction

Cortical activity in awake animals manifests highly complex behavior, often characterized by seemingly noisy activity. At the level of single neurons, the activity in awake animals is associated with considerable subthreshold fluctuations of the membrane potential and irregular firing (Matsumara, Cope, & Fetz, 1988; Steriade, Timofeev, & Grenier, 2001; Destexhe, Rudolph, & Paré, 2003). It is during this regime that the main computational tasks are performed, and understanding those network dynamics is a crucial step toward an analytical study of information processing in neural networks (Destexhe & Contreras, 2006).

Much effort has been devoted to the study of how such activity emerges. Balanced networks have been introduced as a possible model to generate

dynamical states similar to the biological ones (see Figure 1). Two antagonistic states have been highlighted: synchronous regular states (SR) and asynchronous irregular states (AI) (Brunel, 2000). AI states are of particular interest because their dynamical characteristics are very similar to those observed in awake animals. For conductance-based integrate-and-fire neuron networks, they have even been observed without external stimulation (Vogels & Abbott, 2005; El Boustani, Pospischil, Rudolph-Lilith, & Destexhe, 2007; Kumar, Schrader, Aertsen, & Rotter, 2008). Large networks (over 10,000 neurons) are required to yield states consistent with experimental data (El Boustani et al., 2007; Kumar et al., 2008).

In parallel to these studies, population measures of neural activity have also been of great interest, in particular through the emergence of new imaging techniques such as voltage-sensitive dye imaging or two-photon imaging. Although the relation between these signals and single-cell properties is still not completely clear, these measurements reveal structures and correlations over large distances (millimeters or centimeters). No model currently is able to describe neuronal dynamics in large-scale networks at such distance scales, and there is a need for theoretical models specifically designed to handle the temporal and spatial scales of optical imaging.

The type of model that seems most appropriate for such scales are mean-field approaches. Self-consistent mean-field approaches have been proposed and gave predictions about the network stability in a stationary regime (Amit & Brunel, 1997; Brunel, 2000; Latham, Richmond, Nelson, & Nirenberg, 2000; Hertz, Lechner, & Ahmadi, 2004). However, first-order mean-field approximation fails to fully describe these networks because of their inherent dynamics, which can rely dramatically on activity fluctuations. Moreover, the large network limit is usually performed for randomly connected networks despite the lack of biological relevance.

In this letter, our aim is to obtain a macroscopic description of distributed neuronal activity during AI states, where the unit is not the neuron but a small network of neurons. The difficulty, however, is to obtain a description that captures the statistics of network activity while being consistent with single-cell behavior. For this reason, we introduce a mesoscopic description of neuronal activity, in which finite size effects are explicitly taken into account. We consider networks of typical sizes of a few thousand neurons, far away from the large network limit.

To obtain such a mesoscopic model, we use a master equation formalism appropriate for a second-order mean-field description of network activity. The AI states, characterized by low firing rates and exponential decrease of the activity autocorrelation, can be incorporated in such a framework. A complete description of the correlations and covariances can be extracted for timescales governed by the network time constants. Correlations and covariances in the neural dynamics convey crucial information and can be responsible for radical changes in network state according to the parameter regime. This question has already been addressed with a similar formalism

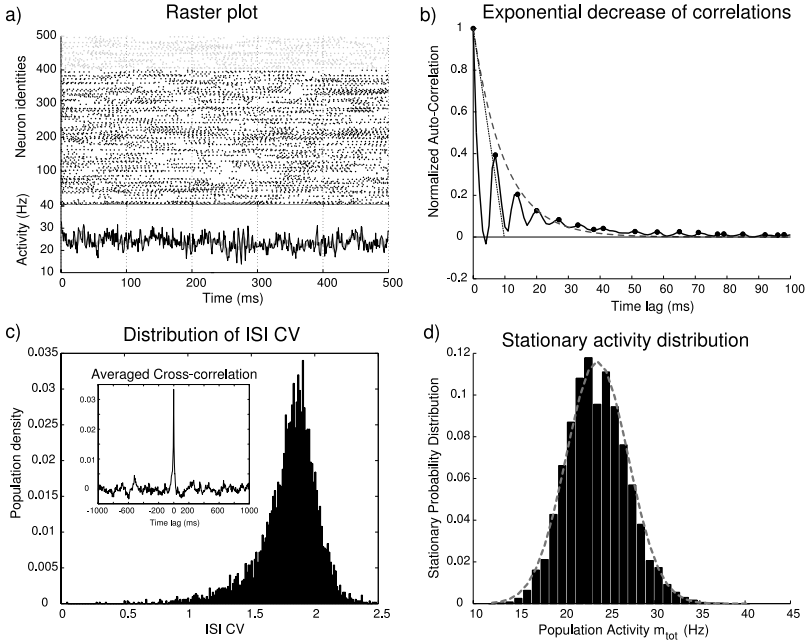


Figure 1: Example of a self-sustained asynchronous irregular (AI) state in a sparsely connected network of conductance-based neurons. The network contains 5000 neurons with a ratio of 4:1 between excitatory and inhibitory neurons and a connection probability $p^{\text{conn}} = 0.01$. Otherwise the neuron model is identical to Vogels and Abbott (2005) with $\Delta g_{\text{exc}} = 7 \text{ nS}$ and $\Delta g_{\text{inh}} = 100 \text{ nS}$. (a) Top: Raster plot for a subset of excitatory (black dots) and inhibitory (gray dots) neurons. Bottom: Population activity with a bin size of 1 ms (black) and 5 ms (gray). The network has a mean activity of 23.68 Hz. (b) Autocorrelation of the total network activity. The dashed gray curve indicates the exponential envelope fit to the autocorrelation positive peaks. The dashed black curve indicates the slope at the origin. The decay time is equal to 10 ms, and the activity has been computed with a bin size of 1 ms. (c) Characterizing the asynchronous irregular state using statistical measures. The population distribution of the interspike interval coefficient of variation (CV) with a mean value of 1.7933, which is higher than 1 for the Poisson process. In the inset, the averaged pairwise cross-correlation computed with a bin size of 5 ms. The value at origin (0.034) estimates the network synchrony. This very low value indicates that there is no substantial synchrony among the neurons. (d) Stationary activity distribution of the network activity. The dashed gray curve indicates the gaussian fit made with the same mean value (23.68 Hz) and standard deviation (3.43 Hz). The activity has been computed with a time bin of 5 ms.

for binary neural networks (Ginzburg & Sompolinsky, 1994; Ohira & Cowan, 1993). Here we intend to develop a more general formalism, applicable to spiking neural networks (El Boustani & Destexhe, 2007).

A similar theory has been studied in parallel (Soula & Chow, 2007) with a discrete description of the network activity. Although a discrete description seems more natural for finite-size networks, several weaknesses appear when considering many populations, which is necessary for networks displaying spontaneously AI states. Indeed, the core of the theory is the transfer function, which maps the output firing rate of the neuron as a function of its synaptic input rates. Theoretical work has been done to obtain analytical transfer functions for a range of neuron models (Tuckwell, 1988; Brunel & Sergi, 1998; Brunel, 2000; Fourcaud & Brunel, 2002; Plesser & Gerstner, 2000). However, to take advantage of such results, we have to rely on a continuous description of network activity to link the neuron statistics to the network ones.

Those computations are not always possible, and a semianalytical approach has been used to tackle this problem (Kumar et al., 2008; Soula & Chow, 2007). In these studies, the neuron transfer function was determined numerically for every network state and used directly for a mean-field approach. This method becomes excessively time-consuming as soon as the network is slightly heterogeneous, which is the case when excitatory and inhibitory neurons have different intrinsic properties, for instance. Indeed, it is necessary to characterize numerically the transfer function for each population and conditionally to every population state. A continuous description is thus necessary to describe heterogeneous networks while benefiting from the theoretical work that has been made at the single-neuron level.

We consider different neuron models ranging from those for which a transfer function has been derived, to those for which an approximative model is required. For the latter, we suggest empirical models that can account for the network dynamics for a broad range of parameters. In particular, for conductance-based neurons, a transfer function can be found that gives a good qualitative description of different network regimes. Those transfer functions are detailed in the next sections and compared with numerical simulations for different model configurations. Finally, to gain some insight into the stability issues of self-sustained AI states and their lifetime, we use second-order statistics to discuss stability in different dynamical regimes, as well as discuss the limits of our approach. A preliminary version of this work has been published previously as a master's thesis (El Boustani, 2006) and a conference abstract (El Boustani & Destexhe, 2007).

2 Methods

All simulations were performed using the NEST simulator (<http://www.nest-initiative.org>) through the PyNN interface (<http://neuralensemble.org/PyNN>). We used different models of AI states in networks of spiking

neurons, based on previous work (Brunel, 2000; Mehring, Hehl, Kubo, Diesmann, & Aertsen, 2003; Vogels & Abbott, 2005). Network size will be 5000 neurons with a ratio of 1:4 between excitatory and inhibitory ($\gamma = \frac{N_{inh}}{N_{tot}} = 0.2$), unless stated otherwise. For current-based models, an event-based strategy (Brette et al., 2007) was used to solve the network equations, and in the conductance-based model, a clock-based strategy was used with a time step of 0.1 ms, which is well beyond every time constant present in the system. In numerical and analytical models, we consider networks without any time delay in synaptic interactions. Based on previous work (Brunel & Hakim, 1999; Brunel, 2000; Vogels & Abbott, 2005), we expect this model to provide a broad range of AI states. In particular, the absence of interaction delay should decrease synchronous regions, as shown in Brunel (2000). Those states will be characterized using the usual statistical measures. To estimate the firing regularity, we will compute the mean interspike interval coefficient of variation. Neuron synchronization will be estimated by computing the mean pairwise cross-correlation among a set of 500 disjoint pairs and at time lag 0. This correlation coefficient is computed with a time bin of 5 ms, which gives a good estimation of synchrony among the neurons (Kumar et al., 2008). The measure is normalized so that it takes values between 0 (no synchrony) and 1 (complete synchrony). Those statistics quantities are illustrated in Figure 1c.

3 Results

We start by describing the general formalism in section 3.1, then consider different neuron models in sections 3.2 and 3.3, and end by illustrating the predictions of this formalism with numerical simulations in section 3.4. The symbol definitions can be found in Table 1 and the simulation parameters in Table 2.

3.1 The Master Equation Formalism. In this section, we develop the mathematical framework in which network dynamics will be described. The mean-field approach has been proven to be a powerful approach to describe networks of spiking neurons if pertinent approximations are done. In previous work, spontaneous activity and networks under stimulation have been studied with self-consistent equations for the neuron stationary mean firing rate (Amit & Brunel, 1997; Brunel, 2000). In these contexts, the individual neuron spike trains are considered as Poisson point processes, which allows one to take into account current fluctuations due to irregular firing. In particular, when a Fokker-Planck approach is used, the membrane potential distribution can be obtained and state diagrams drawn for the network activity. However, once the mean neuron firing rate has been determined, the self-consistent equations are studied without consideration to the population activity fluctuations and temporal dynamics. We propose a framework where a second-order description can be done at the

Table 1: Table of Symbols.

Symbol	Definition	Unit
<i>Network</i>		
N_μ	Number of neuron in population μ	-
γ	Inhibitory/excitatory neuron number ratio	-
$C_{\alpha\mu}$	Number of synaptic input from population α to μ	-
$p_{\alpha\mu}^{conn}$	Proportion of synaptic connection from population α to μ	-
m_μ	Network activity	Hz
m_μ^{ext}	External network activity	Hz
T	Network time constant	ms
<i>Neuron</i>		
v_μ	Transfer function of a neuron in population μ	Hz
V_μ	Membrane potential	mV
V_μ^{rest}	Resting membrane potential	mV
V_μ^{reset}	Firing reset membrane potential	mV
$V_\mu^{threshold}$	Firing threshold potential	mV
R_μ	Input resistance at rest	MΩ
G_μ^L	Leak conductance	nS
C_μ^{mem}	Membrane capacitance	pF
τ_μ^{mem}	Resting membrane time constant	ms
τ_μ^{ref}	Firing refractory period	ms
<i>Synapse</i>		
$A_{\alpha\mu}$	Current synaptic strength from population α to μ	pA
$J_{\alpha\mu}$	Voltage synaptic strength from population α to μ	mV
$\Delta g_{\alpha\mu}$	Conductance synaptic strength from population α to μ	nS
E_α	Reversal potential for the α -type synapse	mV
τ_α	Synaptic time constant for the α -type synapse	ms

population level. In addition to using a stochastic process for the membrane potential, we invoke the master equation to obtain a stochastic process for the network activity using the corresponding neuron transfer function. In AI states, the activity autocorrelation decreases exponentially with the time lag (see Figure 1b), and our main hypothesis is that the network can be modeled as a Markov process for time steps in the order of this decay time.

3.1.1 Main Hypothesis of the Phenomenological Model. Cortical tissue is made of a great variety of neurons, which can be classified according to their biophysical properties. More precisely, electrophysiological measurements can be used to categorize neurons in their contribution to network dynamics. Although those properties exhibit a great diversity, for modeling, we can adopt a stereotypical description where only a few homogeneous populations are considered. In this letter, we consider only two populations, excitatory and inhibitory neurons, but the formalism can accommodate more classes if needed. To keep the model general, we assume that

Table 2: Network Configurations in Numerical Simulations.

Parameter	Value	Unit
γ	0.2	-
T	5 (except Figure 4)	ms
V_μ^{rest}	-60	mV
V_μ^{reset}	-60 (except Figure 5)	mV
$V_\mu^{threshold}$	-50	mV
R_μ	100	$M\Omega$
τ_μ^{mem}	20	ms
τ_μ^{ref}	5	ms
E_{exc}	0	mV
E_{inh}	-80	mV
Figure	N	p^{conn}
2 and 4	5000	0.01
3a	15,000	0.01
3b and 3c	5000–25,000	0.01
1 and 5	5000	0.01
6a–6c	10,000	0.02
6d–6g	5000–10,000	0.01–0.02
7 and 10	10,000	0.01
11	10,000	0.02
12a and 12b	112,500	0.1
12d–12e	10,000	Variable
		(τ_{exc}, τ_{inh})

the network contains K homogeneous populations of neurons, denoted by $1, 2, \dots, K$. We define $m_\gamma(t)$ as the network activity at time t ,

$$m_\gamma(t) = \lim_{\Delta t \rightarrow 0} \frac{n_\gamma(t - \Delta t, t)}{\Delta t N_\gamma}, \quad (3.1)$$

where $n_\gamma(t - \Delta t, t)$ is the number of spikes emitted by population γ during the time interval $[t - \Delta t, t]$ and N_γ is the population size for $\gamma = 1, \dots, K$. In order to build the master equation and obtain the desired Markovian description of network dynamics, we are interested in the conditional probability distribution for a short time interval T ,

$$P(\{m_\gamma(t)\} \mid \{m'_\gamma(t - T)\}), \quad (3.2)$$

with $\gamma = 1, \dots, K$. The system is assumed to be time invariant, so this probability depends only on the time constant T , and we write $P_T(\{m_\gamma\} \mid \{m'_\gamma\})$. This model is eventually intended to describe balanced network dynamics, which are made with sparse connectivity. For large enough networks, this property guarantees the existence of AI states in which pairwise correlations are negligible (van Vreeswijk & Sompolinsky, 1996; Brunel, 2000). We can

thus assume that the population-conditional probabilities are independent from each other beyond the timescale of T :

$$P_T(\{m_\gamma\} \mid \{m'_\gamma\}) = P_T(m_1 \mid \{m'_\gamma\}) \dots P_T(m_K \mid \{m'_\gamma\}). \quad (3.3)$$

Indeed, for a probabilistic system defined through a joint probability distribution, if the random variables are assumed to be independent, this distribution can be factorized in a product of marginal distributions describing each variable exclusively. As the network dynamics is assumed to be memoryless beyond the time interval T , we can then define a Markovian transition operator $W(\{m_\gamma\} \mid \{m'_\gamma\})$ through the continuous master equation for population activities,

$$\begin{aligned} \partial_t P_t(\{m_\gamma\}) &= \prod_{\alpha=1,\dots,K} \int_0^{1/T} dm'_\alpha (P_t(\{m'_\gamma\}) W(\{m_\gamma\} \mid \{m'_\gamma\})) \\ &\quad - P_t(\{m_\gamma\}) W(\{m'_\gamma\} \mid \{m_\gamma\}), \end{aligned} \quad (3.4)$$

where $m_\gamma \in [0, T^{-1}]$ and $\partial_t P_t(\{m_\gamma\})$ is the time derivative of the probability distribution density. In this context, the population activity must be understood as the proportion of neurons that have fired at least once during the last period T , divided by the duration T and not as the instantaneous activity (see equation 3.1). The parameter T controls the temporal resolution of the model, and therefore the activity variables are bound by T^{-1} . However, if T^{-1} is larger than or equal to the neuron maximal firing rate, then we can avoid underestimation of the activity. Indeed, the fastest behavior in the network is defined by the neurons' maximal firing rate. In the SR regime, where excitation prevails over inhibition, the network firing rate is close to the neuron maximal firing rate. However, the time constant T cannot be taken as 0 because significant correlations at this scale would not be considered in this Markovian approach. We aim to describe network states with activity below 50 Hz, which can allow a quite large value for T without the risk of underestimation. An equivalent discrete formalism has been studied by Soula and Chow (2007) with a Markovian approach. Here we insist on keeping a continuous description characterized by the timescale T in order to obtain a framework entirely consistent with the Fokker-Planck approach at the neuron level. The crucial quantity, which must be small to allow this continuous description, is the activity resolution $\Delta m = \frac{1}{NT}$. It describes the minimal change in network activity due to a supplementary spike. It is thus necessary to find a good compromise between network size and time resolution to keep Δm small. The transition operator $W(\{m_\gamma\} \mid \{m'_\gamma\})$ provides the rate of transition from state $\{m'_\gamma\}$ to state $\{m_\gamma\}$ giving the master equation its intuitive interpretation. It can be

defined using the conditional probability density, equation 3.3, by

$$\begin{aligned} W(\{m_\gamma\} \mid \{m'_\gamma\}) &= \lim_{T \rightarrow 0} \frac{P_T(\{m_\gamma\} \mid \{m'_\gamma\})}{T} \\ &= \lim_{T \rightarrow 0} \frac{\prod_{\alpha=1,\dots,K} P_T(m_\alpha \mid \{m'_\gamma\})}{T}. \end{aligned} \quad (3.5)$$

Therefore, we have to compute $P_T(m_\alpha \mid \{m'_\gamma\})$ to fully specify the model. We will adopt a different definition that is more appropriate to our phenomenological model. We assume that the network follows a quasi-stationary evolution, which means that during time T , the system reaches a stationary state, determined by the previous state a time T earlier. This corresponds to the adiabatic hypothesis used in physics. Of course, this approximation no longer holds if the system is stimulated by a signal that possesses frequencies larger than T^{-1} , which can bring the system far from equilibrium. Therefore, and to avoid divergencies due to irrelevant high-order fluctuations, we define the transition function for finite T :

$$W(\{m_\gamma\} \mid \{m'_\gamma\}) = \frac{\prod_{\alpha=1,\dots,K} P_T(m_\alpha \mid \{m'_\gamma\})}{T}. \quad (3.6)$$

Similarly as mentioned before, equation 3.1 is reconsidered for finite T and is bounded by the maximal activity value. Hence, if T is small enough, the master equation formalism can be used. If we consider the limit $T \rightarrow 0$, the activity fluctuations become too important, and the transition function diverges. This parameter is equivalent to the bin size sampling in experiments, and it is well known that bin sizes that are too small give rise to irrelevant fluctuations in the population activity. Furthermore, for an infinitesimal bin size, those fluctuations become punctual, and the transition operator should be reduced to a two-dimensional matrix between the states where the network spikes or does not. To avoid this problem, we require that T has a finite value in the range of the network time constants. The Markovian approach is intended to describe the network dynamics responsible for the activity autocorrelation envelope (see Figure 1b). Correlations' fine structures in the AI regime are caused by residual global oscillations due to finite size effects. However, as the network size increases, the time constant T can take smaller values because the temporal finite-size effect in the autocorrelation vanishes because of sparse connectivity (Brunel, 2000). Thus, we can define a mesoscopic scale for sparsely connected networks in which the network is large enough to avoid temporal correlation finite-size effects but small enough to require second-order statistics to describe its population dynamics. However, the activity autocorrelation decreases exponentially on a timescale of the same order as the system time constants. A Markovian approach should not be acceptable below this timescale, and

we have to choose T carefully according to the regime under consideration. A T that is too large could underestimate the firing rate in high-activity regimes, and T values that are too small will overestimate the second-order statistics. This point has also been discussed in Soula and Chow (2007), but no mention has been made of the fact that the typical autocorrelation fine structure timescales of the network could be smaller than any time constant in the system (Gerstner, 2000), as shown in Figure 1b. Eventually, for a large enough network, we can consider $T = v_{\max}^{-1}$, where v_{\max} is the neuron maximum firing rate, for almost the whole range of the AI regime.

3.1.2 Differential Equations for the Statistical Moments. Using equation 3.4, we can obtain a hierarchy of first-order differential equations for the statistical moments. Indeed, the master equation solution provides the time evolution of the activity probability density. It generally cannot be solved exactly, but one can extract a hierarchy of equations for the statistical moments directly from the differential equation. For balanced networks, this set of equations can be stopped at the second order, and we avoid the closure problem. Indeed, the stationary activity distribution during AI states is well described by a gaussian function when the bin size is not too small (see Figure 1d). This can be understood thanks to the central limit theorem, because we are averaging out higher-order fluctuations during time steps T in the asynchronous activity. Of course, this can hold only if N or T is large enough.

If we close the master equation statistical moments hierarchy to the second order, we get (see appendix A)

$$\begin{aligned}\partial_t \langle m_\mu \rangle &= a_\mu(\{\langle m_\gamma \rangle\}) + \frac{1}{2} \partial_\lambda \partial_\eta a_\mu(\{\langle m_\gamma \rangle\}) c_{\lambda\eta} \\ \partial_t c_{\mu\nu} &= a_{\mu\nu}(\{\langle m_\gamma \rangle\}) + \partial_\lambda a_\mu(\{\langle m_\gamma \rangle\}) c_{\nu\lambda} + \partial_\lambda a_\nu(\{\langle m_\gamma \rangle\}) c_{\mu\lambda},\end{aligned}\tag{3.7}$$

where $\langle m_\mu \rangle$ is the mean population activity and $c_{\mu\nu} = \langle (m_\mu - \langle m_\mu \rangle)(m_\nu - \langle m_\nu \rangle) \rangle$ is the activity covariance matrix. Here and in the following, we use Einstein index summation convention to avoid excessively awkward expressions. If an index is present in only one side of an equality, implicit summation over the whole range of value is understood.

The step moment functions $a_\mu(\{\langle m_\gamma \rangle\})$ and $a_{\mu\nu}(\{\langle m_\gamma \rangle\})$ are defined as follows:

$$\begin{aligned}a_\mu(\{\langle m_\gamma \rangle\}) &= \prod_{\alpha=1,\dots,K} \int_0^{1/T} dm'_\alpha (m'_\mu - \langle m_\mu \rangle) W(\{m'_\gamma\} \mid \{\langle m_\gamma \rangle\}) \\ &= \int_0^{1/T} dm'_\mu (m'_\mu - \langle m_\mu \rangle) \frac{P(m'_\mu \mid \{\langle m_\gamma \rangle\})}{T}\end{aligned}$$

$$\begin{aligned}
a_{\mu\nu}(\{\langle m_\gamma \rangle\}) &= \prod_{\alpha=1,\dots,K} \int_0^{1/T} dm'_\alpha (m'_\mu - \langle m_\mu \rangle) \\
&\quad \times (m'_v - \langle m_v \rangle) W(\{m'_\gamma\} \mid \{\langle m_\gamma \rangle\}) \\
&= \int_0^{1/T} dm'_\mu \int_0^{1/T} dm'_v (m'_\mu - \langle m_\mu \rangle) (m'_v - \langle m_v \rangle) \\
&\quad \times \frac{P(m'_\mu \mid \{\langle m_\gamma \rangle\}) P(m'_v \mid \{\langle m_\gamma \rangle\})}{T}.
\end{aligned} \tag{3.8}$$

The second and last identity has been obtained by using equation 3.5 given by the independence hypothesis. To complete the second-order development, we need to describe the correlation matrix of the network $\text{Corr}_{\mu\nu}(t, t + \tau) = \langle (m_\mu(t) - \langle m_\mu(t) \rangle)(m_\nu(t + \tau) - \langle m_\nu(t + \tau) \rangle) \rangle$. This is done in appendix B, and the resulting differential equation for a stationary state is given by

$$\partial_\tau \text{Corr}_{\mu\nu}(\tau) = \partial_\lambda a_\nu(\{m_\gamma^{stat}\}) \text{Corr}_{\mu\lambda}(\tau), \tag{3.9}$$

where $a_\nu(\{\langle m_\gamma \rangle\})$ is defined in equation 3.8 and $\{m_\gamma^{stat}\}$ is a the stationary solution of the set in equation 3.7.

3.1.3 A Model for the Transition Function. Finally, to complete this framework, we need to specify the transition functions $W(m_\alpha \mid \{m'_\gamma\})$ for $\alpha = 1, \dots, K$. These functions depend directly on the neuron properties. When a neuron is part of network dynamics and is exposed to intense synaptic inputs, it can be described using a transfer function that maps the neuron output firing rate to the synaptic inputs, regardless of their origin. In a recurrent neuron network, the synaptic input is provided by other neurons in the network and thus depends on the network activity. If we assume that we know the stationary transfer function of neurons in population α , v_α , then the probability p_α that a neuron in this population fires during time T given the previous state of the network $\{m'_\gamma\}$ is

$$p_\alpha(\{m'_\gamma\}) \simeq v_\alpha(\{m'_\gamma\}) T \leq 1.$$

This is a direct consequence of the adiabatic hypothesis we made in section 3.1.1. Indeed, the network in its previous state is characterized by a stationary transfer function so that the network activity is assumed to evolve near stationary states. During time T , each neuron can fire only once, so that we can express for the population α the desired conditional probability $P_T(m_\alpha \mid \{m'_\gamma\})$ with a binomial distribution using the independence

hypothesis,

$$P_T(m_\alpha \mid \{m'_\gamma\}) = \binom{N_\alpha}{m_\alpha N_\alpha T} p_\alpha(\{m'_\gamma\})^{m_\alpha N_\alpha T} (1 - p_\alpha(\{m'_\gamma\}))^{N_\alpha(1-m_\alpha T)}, \quad (3.10)$$

where it is implicitly understood that we take the integer part of $m_\alpha N_\alpha T$. However, as population size N_α increases, the correction due to the noninteger part becomes negligible, and we can apply the gaussian approximation by using the Stirling formula $n! \sim \sqrt{2\pi n^{(n+1/2)}} e^{-n}$, leading to

$$\begin{aligned} P_T(m_\alpha \mid \{m'_\gamma\}) &\simeq \sqrt{\frac{N_\alpha}{2\pi v_\alpha(\{m'_\gamma\})(1/T - v_\alpha(\{m'_\gamma\}))}} \\ &\times \exp \left[-N_\alpha \frac{(m_\alpha - v_\alpha(\{m'_\gamma\}))^2}{2v_\alpha(\{m'_\gamma\})(1/T - v_\alpha(\{m'_\gamma\}))} \right]. \end{aligned} \quad (3.11)$$

We see that this population conditional probability density follows a normal law with a variance that decreases when the neuron firing rate is near saturation $v_\alpha = 1/T$ or in a quiescent state $v_\alpha = 0$. If symmetries are broken in the population α and the neurons are not identical, this law is no longer valid. However, this law is a good first approximation because if the neuron firing rate in the population α follows a particular distribution due to slight heterogeneities and N_α are big enough, then the central limit theorem implies that the activity distribution is well described by a normal law with the same mean value. In this case, this mean value is the neuron transfer function in population α , formally v_α . Furthermore, the more N_α increases, the narrower the normal distribution becomes. Thus, the theory describes large networks but also accounts for finite-size effects and is therefore close to a “mesoscopic” description. Indeed, if $\{N_\alpha\}$ is taken to infinity, the normal law tends to a Dirac function in the sense of distribution theory. If T is kept constant while the network size is taken to infinity, the first-order mean field is recovered because fluctuations are completely averaged out and the second-order development is irrelevant. This phenomenological model stays in accordance with numerical models as long as T is kept finite. We finally get the transition function by dividing the conditional probability by T according to definition 3.6,

$$\begin{aligned} W(\{m_\gamma\} \mid \{m'_\gamma\}) \\ = \frac{1}{T} \sqrt{\frac{\det(A)}{(2\pi)^K}} \exp \left[-\frac{1}{2} (m_\mu - v_\mu(\{m'_\gamma\})) A_{\mu\nu} (m_\nu - v_\nu(\{m'_\gamma\})) \right], \end{aligned} \quad (3.12)$$

where $A_{\mu\nu} = \delta_{\mu\nu} \frac{N_\mu}{v_\mu(\langle m'_\nu \rangle)(1/T - v_\mu(\langle m'_\nu \rangle))}$. The integral of this transition function over the entire state space gives trivially $\frac{1}{T}$, which can now be roughly interpreted as the degree of fluctuation taken into account. Indeed, if $T \rightarrow \infty$, the total integral goes to 0, which means that we are in the first-order mean-field approximation and the variance has no meaning, whereas if $T \rightarrow 0$, the total integral goes to infinity, which means that infinitesimal fluctuations are taken into account. These fluctuations are not relevant in our framework, and we keep $T \sim v_{\max}^{-1}$. If the interneuron correlations become substantial, the independence hypothesis no longer holds, and we have to consider another model to replace the binomial transition function. For large, sparsely connected networks, however, the independence hypothesis gives accurate results.

The whole formalism is completely described by the transition function, equation 3.12. The set of equations for the first- and second-order statistical moments can be further specified by injecting this transition function in the functions 3.8. We integrate over the complete real line because equation 3.12 is centered on $0 < v_\alpha < T^{-1}$ with a variance that vanishes at the boundaries, so that the corrective terms are of order $\mathcal{O}(e^{-N})$ and can be ignored for large enough populations. This is a natural consequence of the gaussian approximation. We then obtain

$$\begin{aligned} a_\mu(\{\langle m_\gamma \rangle\}) &= \frac{1}{T} \int_{-\infty}^{\infty} dm'_\mu (m'_\mu - \langle m_\mu \rangle) P(m'_\mu \mid \{\langle m_\gamma \rangle\}) \\ &= \frac{1}{T} (v_\mu - \langle m_\mu \rangle) \end{aligned} \quad (3.13)$$

$$\begin{aligned} a_{\mu\nu}(\{\langle m_\gamma \rangle\}) &= \int_{-\infty}^{\infty} dm'_\mu \int_{-\infty}^{\infty} dm'_v (m'_\mu - \langle m_\mu \rangle) \\ &\quad \times (m'_v - \langle m_v \rangle) W(\{m'_\gamma\} \mid \{\langle m_\gamma \rangle\}) \\ &= \frac{\delta_{\mu\nu}}{T} \int_{-\infty}^{\infty} dm'_\mu (m'^2_\mu - v_\mu^2 + v_\mu^2 - 2m'_\mu \langle m_\mu \rangle \\ &\quad + \langle m_\mu \rangle^2) P(m'_\mu \mid \{\langle m_\gamma \rangle\}) \\ &\quad + \frac{(1 - \delta_{\mu\nu})}{T} (v_\mu - \langle m_\mu \rangle)(v_v - \langle m_v \rangle) \\ &= \frac{1}{T} \left(\delta_{\mu\nu} \frac{v_\mu(1/T - v_\mu)}{N_\mu} + (v_\mu - \langle m_\mu \rangle)(v_v - \langle m_v \rangle) \right) \\ &= \frac{1}{T} (\delta_{\mu\nu} A_{\mu\mu}^{-1} + T^2 a_\mu a_v), \end{aligned} \quad (3.14)$$

where $v_\mu = v_\mu(\{\langle m_\gamma \rangle\})$ is the transfer function of a neuron in the population μ , which depends on the mean activity of every population. To get

every term in equation 3.7, we need to differentiate equation 3.13. The corresponding functions and derivatives give

$$\begin{aligned} a_\mu(\{\langle m_\gamma \rangle\}) &= \frac{1}{T} (v_\mu - \langle m_\mu \rangle) \\ \partial_\lambda a_\mu(\{\langle m_\gamma \rangle\}) &= \frac{1}{T} (\partial_\lambda v_\mu - \delta_{\mu\lambda}) \\ \partial_\lambda \partial_\eta a_\mu(\{\langle m_\gamma \rangle\}) &= \frac{1}{T} \partial_\lambda \partial_\eta v_\mu. \end{aligned} \quad (3.15)$$

Equations 3.7, 3.15, 3.9, and 3.14 provide a complete description of this master equation formalism, and we can write the set of differential equations according to those functions:

$$T \partial_t \langle m_\mu \rangle = (v_\mu - \langle m_\mu \rangle) + \frac{1}{2} \partial_\lambda \partial_\eta v_\mu c_{\lambda\eta} \quad (3.16)$$

$$\begin{aligned} T \partial_t c_{\mu\nu} &= \delta_{\mu\nu} A_{\mu\mu}^{-1} + (v_\mu - \langle m_\mu \rangle)(v_\nu - \langle m_\nu \rangle) \\ &\quad + \partial_\lambda v_\mu c_{\nu\lambda} + \partial_\lambda v_\nu c_{\mu\lambda} - 2c_{\mu\nu} \end{aligned}$$

$$T \partial_\tau \text{Corr}_{\mu\nu}(\tau) = (\partial_\lambda v_\nu(\{\langle m_\gamma^{stat} \rangle\}) - \delta_{\lambda\nu}) \text{Corr}_{\mu\lambda}(\tau) \quad (3.17)$$

We see that the determinant function for the first-order differential equation is the transfer function itself, which can be expected from the usual first-order analysis. The second-order statistics (covariances and correlations) are led mainly by the first derivative of the transfer function. We can expect higher-order statistical moments to depend on higher-order derivatives of this function in this framework. Thus, the set of transfer function $\{v_\alpha\}$ for $\alpha = 1, \dots, K$ plays a crucial role and should be determined to complete the model. In the next section, we consider different models.

3.2 The Linear Model. In this section, we illustrate some aspect of this master equation formalism, which could be harder to analyze once it is used for more realistic transfer functions. Following Soula and Chow (2007), we treat the simple case of a linear transfer function for a network of excitatory and inhibitory cells. Every neuron has the same transfer function (homogeneous intrinsic properties):

$$v(\{m_\gamma\}) = v_0 + k_{exc} m_{exc} + k_{inh} m_{inh}. \quad (3.18)$$

This problem is similar to a balanced network where all neurons receive the same synaptic input and have the same transfer function. In this case, the differential equations for the mean activities do not depend on the second-order moments. The set of second-order differential equations 3.16, can

thus be written with equation 3.15:

$$T \partial_t \langle m_\mu \rangle = v_0 + k_{exc} \langle m_{exc} \rangle + k_{inh} \langle m_{inh} \rangle - \langle m_\mu \rangle \quad (3.19)$$

$$\begin{aligned} T \partial_t c_{\mu\nu} &= \frac{\delta_{\mu\nu}}{N_\mu} v(T^{-1} - v) + (v - \langle m_\mu \rangle)(v - \langle m_\nu \rangle) \\ &\quad + k_\lambda c_{\mu\lambda} + k_\lambda c_{\nu\lambda} - 2c_{\mu\nu}. \end{aligned} \quad (3.20)$$

This set of equations is linear, and we can look for the fixed point of the mean activity, equation 3.19, first. The solution of the linear system gives

$$m_0 = \langle m_{exc}^{FP} \rangle = \langle m_{inh}^{FP} \rangle = \frac{v_0}{1 - \Delta}, \quad (3.21)$$

where $\Delta = k_{exc} + k_{inh}$ is the transfer function slope, which is modulated by excitatory and inhibitory strengths. The stability of this fixed point is given by the eigenvalues of the linear system, and we get the following values:

$$\lambda_1 = -1$$

$$\lambda_2 = \Delta - 1,$$

and we see as expected that the two populations converge to a common fixed point, whereas this fixed-point stability depends on the total slope Δ , which must be inferior to unity. We can now study the remaining equations for the second-order moments 3.20. With the fixed-point 3.21, the system reduced to a simple set of three linear equations, which gives the fixed-point value for the covariance matrix. The solution is given by the following form:

$$\begin{aligned} \sigma^2(m_{exc})^{FP} &= \frac{m_0(1/T - m_0)}{2(\Delta - 2)(\Delta - 1)} \\ &\times \left(\frac{(\Delta - 2)(1 - \Delta) + k_{exc}k_{inh}(k_{inh} - 1)}{(k_{exc} - 1)N_{exc}} + \frac{k_{inh}^2}{N_{inh}} \right) \\ \sigma^2(m_{inh})^{FP} &= \frac{m_0(1/T - m_0)}{2(\Delta - 2)(\Delta - 1)} \\ &\times \left(\frac{k_{exc}^2}{N_{exc}} + \frac{(\Delta - 2)(1 - \Delta) + k_{inh}k_{exc}(k_{exc} - 1)}{(k_{inh} - 1)N_{inh}} \right) \\ c_{exc/inh}^{FP} &= -\frac{m_0(1/T - m_0)}{2(\Delta - 2)(\Delta - 1)} \left(\frac{k_{exc}(k_{inh} - 1)}{N_{exc}} + \frac{k_{inh}(k_{exc} - 1)}{N_{inh}} \right). \end{aligned} \quad (3.22)$$

Again we have to compute the eigenvalues of this linear system to study this fixed-point stability. We get

$$\begin{aligned}\lambda_3 &= -2 \\ \lambda_4 &= 2(\Delta - 1) \\ \lambda_5 &= \Delta - 2.\end{aligned}$$

Those values guarantee the coherence in the covariance matrix. Nothing is learned about the network stability that was not already deduced from the mean activity set of equations. There is only a need for a balanced activity such that $\Delta < 1$ to avoid the system's exploding. However, one has to remember that the fixed point is described with its fluctuations, so transitions between states are not excluded in a more complex system. We see from the set 3.22 that the covariance matrix entries decrease with the network size, and eventually we recover the first-order mean field when the networks are large enough, which is not the case with a description in terms of the number of spiking neurons. This relation is not exactly observed in small networks (Soula & Chow, 2007) due to a strong pairwise correlation, but if the network size is increased to biophysical scales, the relation is quite correct (Kumar et al., 2008). For finite-size networks, excitatory and inhibitory variances are different when sizes are different, even though the mean activity has exactly the same value in the stationary regime. Similar to Soula and Chow (2007), the network displays large fluctuations when it operates near the critical point $\Delta = 1$. Here again, we see that a description in terms of activity gives a unified description between neurons and networks where the limit $N \rightarrow \infty$ is well defined. We give the correlation matrix (see equation B.5) to finish the example:

$$T \partial_\tau \text{Corr}_{\mu\nu}(\tau) = (\partial_\lambda v(\{m_\gamma^{FP}\}) - \delta_{\nu\lambda}) \text{Corr}_{\mu\lambda}(\tau) \quad (3.23)$$

$$= k_{exc} \text{Corr}_{\mu/exc}(\tau) + k_{inh} \text{Corr}_{\mu/inh}(\tau) - \text{Corr}_{\mu\nu}(\tau), \quad (3.24)$$

for which the eigenvalues are easily determined, and we find the same values as for the mean activity λ_1 and λ_2 with an algebraic multiplicity of 2. They describe the decrease of autocorrelation and cross-correlation. We see here again that $\Delta = 1$ corresponds to a critical point where correlations are infinite spatially (between population activities) and temporally (within population activities).

3.3 Spiking Network Models.

3.3.1 Network Structure. Chaotic spontaneous activity as well as an asynchronous irregular regime have been observed in sparsely connected networks (Brunel, 2000; Brunel & Hakim, 1999; Kumar et al., 2008; van

Vreeswijk & Sompolinsky, 1996, 1998; Mehring et al., 2003; Vogels & Abbott, 2005). Sparse connections have been shown to be crucial to provide the network's irregular behavior. However, the connections do not need to be purely random (Mehring et al., 2003). A degree of locality in the connections can be tolerated as long as the correlations between neurons do not become critically strong and destroy the chaotic activity. We will consider sparsely connected networks with random connectivity. We will show in the numerical simulations that the model can still give good predictions when the neurons are locally sparsely connected. For the moment, every neuron from population μ receives randomly $C_{\alpha\mu}$ synaptic input from population α where $\frac{C_{\alpha\mu}}{N_\alpha} = p_{\alpha\mu}^{\text{conn}} < 1$. Usually $p_{\alpha\mu}^{\text{conn}}$ is taken between 1% and 10%.

3.3.2 Current-Based Integrate-and-Fire Neurons. We will consider current-based integrate-and-fire (IAF) neurons with the corresponding membrane potential equation,

$$\tau_\mu^{\text{mem}} \frac{d}{dt} V_{i_\mu}(t) = - (V_{i_\mu}(t) - V_\mu^{\text{rest}}) + R_\mu I_{i_\mu}(t) \quad \mu \in [0, K] \quad \text{and} \quad i_\mu \in [0, N_\mu], \quad (3.25)$$

where V_μ^{rest} is the resting potential and R_μ and τ_μ^{mem} are, respectively, the membrane resistance and time constant of neurons in the population μ . If the threshold $V_\mu^{\text{threshold}}$ is crossed, the neuron emits a spike, and the membrane potential is clamped to the reset potential V_μ^{reset} during a refractory period τ_μ^{ref} . $I_{i_\mu}(t)$ is the external current coming from other neurons in the network $I_{i_\mu}^{\text{int}}(t)$ or from an external source $I_{i_\mu}^{\text{ext}}(t)$. Because each population is homogeneous, we write μ instead of i_μ to simplify the notation.

To build the transition function, we have used a binomial law based on the independence approximation on timescale T . However, nothing was specified on the temporal structure of the spike trains emitted by each population during this timescale. If we assume the classical Poisson model for each neuron, the entire population can be modeled as a Poisson process too. The internal contribution is then represented as the convolution between a Poisson spike train and a postsynaptic potential function $PSP_{\alpha\mu}(t)$ from population α to population μ ,

$$R_\mu I_\mu^{\text{int}}(t) = \sum_{\alpha=1, \dots, K} \int_{\mathbb{R}} PSP_{\alpha\mu}(t-s) N_{\alpha\mu}(ds), \quad (3.26)$$

where $N_{\alpha\mu}(ds)$ are Poisson point processes describing the incoming spike trains. We discuss different synapse functions in the next section. We consider external stimulation currents also as Poisson spike trains with rate m_α^{ext} .

One of the advantages of a description in term of continuous activity is that we can benefit from the Fokker-Planck approach to compute different transfer functions for our neurons. Although neurons can have different firing rates during the dynamics, we consider that, independently for every population, the law of large numbers prevails after time T , and only the mean firing rate of the whole process should be considered. Therefore, if we have $C_{\alpha\mu}$ incoming spike trains from population α to population μ with a mean firing rate m_α , then the total spike train can be considered a Poisson process of total rate $C_{\alpha\mu}m_\alpha$. Using the diffusion approximation, we can deduce the free (without spike mechanism) membrane potential distribution. This can be used as a first approximation to estimate the neuron transfer function (Amit & Brunel, 1997). Once the Fokker-Planck solution $P_\mu(V)$ is found, we consider that the output firing rate is given by the distribution tail that lies above the threshold divided by the membrane time constant:

$$\nu_\mu = \frac{1}{\tau_\mu^{mem}} \int_{V_\mu^{threshold}}^{\infty} dVP(V) = \frac{1}{2\tau_\mu^{mem}} \left(1 + erf \left(\frac{\langle V_\mu \rangle - V_\mu^{threshold}}{\sqrt{2}\sigma(V_\mu)} \right) \right). \quad (3.27)$$

This approximation is valid as long as the membrane time constant leads the dynamics, more specifically in the AI regime. If the spike mechanism is included in the Fokker-Planck approach, an exact solution can be obtained for some synapse type for the IAF neuron transfer function. Brunel (2000) showed that for instantaneous synapses (Dirac functions), the solution is given by the inverse mean interspike interval of the first passage problem with white noise (Tuckwell, 1988). More recently (Fourcaud & Brunel, 2002), a correction has been added to take into account the colored noise produced by exponential synapses as long as the ratio $\sqrt{\frac{\tau_{syn}}{\tau_\mu^{mem}}}$ is small compared to unity. The transfer function for this first-order correction is similar to the one used in Brunel (2000) but with a corrective term $\Delta h_\mu \sim 1.03\sqrt{\frac{\tau_{syn}}{\tau_\mu^{mem}}}$,

$$\nu_\mu = \left(\tau_\mu^{ref} + \tau_\mu^{mem} \sqrt{\pi} \int_{\frac{V_\mu^{reset} - \langle V_\mu \rangle}{\sqrt{2}\sigma(V_\mu)} + \Delta h_\mu}^{\frac{V_\mu^{threshold} - \langle V_\mu \rangle}{\sqrt{2}\sigma(V_\mu)} + \Delta h_\mu} du e^{u^2} (1 + erf(u)) \right)^{-1}, \quad (3.28)$$

where the membrane potential statistics are given by the white noise model and the new synaptic weights must be normalized to ensure the correspondence between exponential synapses and Dirac synapses when the synaptic time constants are taken to 0. We have the following relation, $J_\alpha^{Dirac} = J_\alpha^{Exp} \frac{\tau_\alpha}{\tau_\mu^{mem}}$, where J_α and τ_α are the synaptic strength and time constant corresponding to synapse α . If we consider a balanced network made of excitatory and inhibitory neurons, the largest synaptic time constant will mainly be responsible for the corrective term. In all simulations presented

here, the inhibitory synaptic time constant will be at least twice as large as the excitatory time constant, so that the corrective term must be of the order $\Delta h_\mu \sim 1.03 \sqrt{\frac{V_{inh}}{\tau_\mu^{mem}}}$. However, in the following, we will consider network models where the synaptic time constant can be large compared to the membrane time constant (Vogels & Abbott, 2005), so we decided to adopt a different model for the transfer function. Instead of using the membrane potential mean value and variance computed with white noise, we will use shot noise processes to deduce those values for different synapses and replace $\langle V_\mu \rangle$ and $\sigma^2(V_\mu)$ in the transfer function, equation 3.28, without the corrective term:

$$v_\mu = \left(\tau_\mu^{ref} + \tau_\mu^{mem} \sqrt{\pi} \int_{\frac{V_\mu^{reset} - \langle V_\mu \rangle}{\sqrt{2\sigma(V_\mu)}}}^{\frac{V_\mu^{threshold} - \langle V_\mu \rangle}{\sqrt{2\sigma(V_\mu)}}} du e^{u^2} (1 + erf(u)) \right)^{-1}. \quad (3.29)$$

The mean membrane potential $\langle V_\mu \rangle$ and the variance $\sigma^2(V_\mu)$ depend on the incoming activity and the chosen synapse. This point is discussed in the next section, where different types of synapses are considered. As long as the model allows, we can also estimate the coefficient of variation of the interspike interval by using the recurrence relation developed for the first-passage problem (Tuckwell, 1988). For the model introduced in Brunel (2000), this quantity is given in a stationary point by

$$\begin{aligned} CV_\mu^2 = & 2\pi (\tau_\mu^{mem} \langle m_\mu \rangle^{stat})^2 \int_{\frac{V_\mu^{reset} - \langle V_\mu \rangle^{stat}}{\sigma(V_\mu)^{stat}}}^{\frac{V_\mu^{threshold} - \langle V_\mu \rangle^{stat}}{\sigma(V_\mu)^{stat}}} dx e^{x^2} \\ & \times \int_{-\infty}^x dy e^{y^2} (1 + erf(y))^2. \end{aligned} \quad (3.30)$$

It is thus possible to access second-order statistics at the single-neuron level as well as the network level as long as the neuron model is specified. This is a powerful aspect of this theory, and it will play a crucial role in applying this framework to the study of voltage-sensitive dyes optical imaging data. Indeed, this type of signal is proportional to the subthreshold membrane potential, and we need a simple dynamic description that can give us access to the membrane potential distribution. This is done on timescales T with the network activity differential equation. Therefore, it is necessary to have a description at both levels. The formal equation for the interspike interval coefficient of variation (ISI CV) is not always determined, however, Kumar et al. (2008) noticed that the activity variance is very informative on the spiking regularity for self-sustained balanced networks. In some cases, the activity variance could describe the firing irregularity without the need for an exact equation for ISI CV. The limitation in the analytical derivation of the transfer function and the ISI CV depends on the chosen synapse or, equivalently, the nature of correlation in the current input. In the next section, we present different kind of synapses, some of which allow exact analytical results.

Synapse models. In the preceding section, we mentioned the Fokker-Planck approach. We need to determine the relation between the incoming spike train statistics and the membrane potential probability distribution. In particular, it is necessary to compute the mean and the variance according to the firing rate. Under the Poisson approximation, shot noise theory provides the required relations through Campbell's theorem,

$$\langle V_\mu \rangle = V_\mu^{rest} + \sum_{\alpha=1,\dots,K} C_{\alpha\mu} (m_\alpha + m_\alpha^{ext}) \int_{\mathbb{R}} dt PSP_{\alpha\mu}(t) \quad (3.31)$$

$$\sigma^2(V_\mu) = \sum_{\alpha=1,\dots,K} C_{\alpha\mu} (m_\alpha + m_\alpha^{ext}) \int_{\mathbb{R}} dt PSP_{\alpha\mu}^2(t), \quad (3.32)$$

where $PSP_{\alpha\mu}(t)$ with $\alpha, \mu \in \{1, \dots, K\}$ are the membrane potential time courses elicited by population α synapses on population μ . We will consider different synapse functions and compute these functions using equation 3.25, which is exactly solvable.

- *Dirac synapses (instantaneous).* Our first model is the Dirac synapse current,

$$syn_{\alpha\mu}(t) = A_{\alpha\mu} \tau_\mu^{mem} \delta(t),$$

with $A_{\alpha\mu}$ the synaptic strength. Once integrated through equation 3.25, the membrane potential equation, this synapse gives the following postsynaptic potential,

$$PSP_{\alpha\mu}(t) = R_\mu A_{\alpha\mu} e^{-t/\tau_\mu^{mem}} H(t),$$

where $H(t)$ is the Heaviside function. Using equations 3.31 and 3.32, we finally get the desired statistics characteristics,

$$\begin{aligned} \langle V_\mu \rangle &= V_\mu^{rest} + \tau_\mu^{mem} \sum_{\alpha=1,\dots,K} J_{\alpha\mu} C_{\alpha\mu} (m_\alpha + m_\alpha^{ext}) \\ \sigma^2(V_\mu) &= \frac{1}{2} \sum_{\alpha=1,\dots,K} \tau_\mu^{mem} J_{\alpha\mu}^2 C_{\alpha\mu} (m_\alpha + m_\alpha^{ext}), \end{aligned} \quad (3.33)$$

with $J_{\alpha\mu} = R_\mu A_{\alpha\mu}$ the potential increment.

- *Exponential synapses.* A more realistic model would include a decaying tail to the synaptic current with a time constant specific to each synapse type. The next step in modeling realistic synapses is the exponential synapse model,

$$syn_{\alpha\mu}(t) = A_{\alpha\mu} e^{-t/\tau_\alpha} H(t)$$

$$PSP_{\alpha\mu}(t) = \frac{J_{\alpha\mu} \tau_\alpha}{\tau_\mu^{mem} - \tau_\alpha} (e^{-t/\tau_\mu^{mem}} - e^{-t/\tau_\alpha}) H(t),$$

where τ_α is the decay time constant for synapses coming from the population α , so that we finally get

$$\begin{aligned}\langle V_\mu \rangle &= V_\mu^{rest} + \sum_{\alpha=1,\dots,K} J_{\alpha\mu} \tau_\alpha C_{\alpha\mu} (m_\alpha + m_\alpha^{ext}) \\ \sigma^2(V_\mu) &= \frac{1}{2} \sum_{\alpha=1,\dots,K} \frac{J_{\alpha\mu}^2 \tau_\alpha^2}{\tau_\alpha + \tau_\mu^{mem}} C_{\alpha\mu} (m_\alpha + m_\alpha^{ext}).\end{aligned}\quad (3.34)$$

- α -synapses. To include a finite rising time of the synaptic current, we use alpha functions, which correspond to the following forms:

$$\begin{aligned}syn_{\alpha\mu}(t) &= A_{\alpha\mu} \frac{t}{\tau_\alpha} e^{1-t/\tau_\alpha} H(t) \\ PSP_{\alpha\mu}(t) &= J_{\alpha\mu} e \left(\frac{-te^{-t/\tau_\alpha}}{\tau_\mu^{mem} - \tau_\alpha} + \frac{\tau_\mu^{mem} \tau_\alpha}{(\tau_\mu^{mem} - \tau_\alpha)^2} (e^{-t/\tau_\mu^{mem}} - e^{-t/\tau_\alpha}) \right) H(t)\end{aligned}$$

and

$$\begin{aligned}\langle V_\mu \rangle &= V_\mu^{rest} + e \sum_{\alpha=1,\dots,K} J_{\alpha\mu} \tau_\alpha C_{\alpha\mu} (m_\alpha + m_\alpha^{ext}) \\ \sigma^2(V_\mu) &= \sum_{\alpha=1,\dots,K} (2\tau_\mu^{mem} + \tau_\alpha) \left(\frac{e J_{\alpha\mu} \tau_\alpha}{2(\tau_\mu^{mem} + \tau_\alpha)} \right)^2 C_{\alpha\mu} (m_\alpha + m_\alpha^{ext}).\end{aligned}\quad (3.35)$$

Neuron transfer function in the master equation. Now that we have specified the membrane potential mean value and variance, we have to incorporate these functions in the neuron transfer function to derive the network dynamics equations. We compute the necessary functions using the free membrane potential transfer function, as well as the phenomenological transfer function defined with the Campbell's theorem in the previous section. We thus use the definitions—equation 3.27 or 3.29 into 3.15—to get a complete description of the set of differential equations. We make some definitions to simplify the computation for equation 3.27,

$$\begin{aligned}Q_\mu &= \langle V_\mu \rangle - V_\mu^{threshold} \\ &= \Phi_{\alpha\mu} (m_\alpha + m_\alpha^{ext}) + (V_\mu^{rest} - V_\mu^{threshold}),\end{aligned}\quad (3.36)$$

where $\Phi_{\alpha\mu}$ depends on the chosen synapses,

$$\Phi_{\alpha\mu}^{Dirac} = \tau_\mu^{mem} J_{\alpha\mu} C_{\alpha\mu} \quad \Phi_{\alpha\mu}^{Exp} = \tau_\alpha J_{\alpha\mu} C_{\alpha\mu} \quad \Phi_{\alpha\mu}^{asym} = e \tau_\alpha J_{\alpha\mu} C_{\alpha\mu}, \quad (3.37)$$

and similarly

$$\begin{aligned}K_\mu &= 2\sigma^2(V_\mu) \\ &= \Psi_{\alpha\mu} (m_\alpha + m_\alpha^{ext}),\end{aligned}\quad (3.38)$$

with the corresponding synapse functions,

$$\begin{aligned}\Psi_{\alpha\mu}^{Dirac} &= \tau_\mu^{mem} J_{\alpha\mu}^2 C_{\alpha\mu} & \Psi_{\alpha\mu}^{Exp} &= \frac{J_{\alpha\mu}^2 \tau_\alpha^2}{\tau_\alpha + \tau_\mu^{mem}} C_{\alpha\mu} \\ \Psi_{\alpha\mu}^{\alpha syn} &= \frac{(2\tau_\mu^{mem} + \tau_\alpha)}{2} \left(\frac{e J_{\alpha\mu} \tau_\alpha}{(\tau_\mu^{mem} + \tau_\alpha)} \right)^2 C_{\alpha\mu},\end{aligned}\quad (3.39)$$

such that the transfer function, equation 3.27, can be written as

$$v_\mu = \frac{1}{2\tau_\mu^{mem}} \left(1 + \operatorname{erf} \left(\frac{Q_\mu}{\sqrt{K_\mu}} \right) \right). \quad (3.40)$$

To obtain the full set of differential equations, equation 3.16, we need to compute the step function derivatives, equation 3.15,

$$\partial_\lambda a_\mu(\{m_\gamma\}) = \frac{1}{T} \left(\frac{e^{-\frac{Q_\mu^2}{K_\mu}}}{\sqrt{\pi} \tau_\mu^{mem}} \left(\frac{2K_\mu \Phi_{\lambda\mu} - Q_\mu \Psi_{\lambda\mu}}{2K_\mu^{3/2}} \right) - \delta_{\lambda\mu} \right)$$

and for the second derivative,

$$\begin{aligned}\partial_\lambda \partial_\eta a_\mu(\{m_\gamma\}) &= \frac{e^{-\frac{Q_\mu^2}{K_\mu}}}{\sqrt{\pi T} \tau_\mu^{mem}} \\ &\cdot \left(\frac{2K_\mu (2Q_\mu^2 - K_\mu) (\Phi_\lambda \Psi_\eta + \Phi_\eta \Psi_\lambda) + Q_\mu (3K_\mu - 2Q_\mu^2) \Psi_\lambda \Psi_\eta - 8K_\mu^2 Q_\mu \Phi_\lambda \Phi_\eta}{4K_\mu^{7/2}} \right).\end{aligned}$$

If we consider the transfer function, equation 3.29, we have to define slightly different functions,

$$\begin{aligned}Q_\mu^{th} &= V_\mu^{threshold} - (V_\mu^{rest} + \Phi_{\alpha\mu}(m_\alpha + m_\alpha^{ext})) \\ Q_\mu^{re} &= V_\mu^{reset} - (V_\mu^{rest} + \Phi_{\alpha\mu}(m_\alpha + m_\alpha^{ext})) \\ K_\mu &= \Psi_{\alpha\mu}(m_\alpha + m_\alpha^{ext}),\end{aligned}\quad (3.41)$$

where $\Phi_{\alpha\mu}$ and $\Psi_{\gamma\mu}$ depend on the chosen synapses and are defined as previously. We also define

$$\begin{aligned}x_\mu^{th} &= \frac{Q_\mu^{th}}{\sqrt{K_\mu}} \\ x_\mu^{re} &= \frac{Q_\mu^{re}}{\sqrt{K_\mu}}\end{aligned}$$

such that equation 3.29 can be written in a shorter form:

$$\nu_\mu = \left(\tau_\mu^{ref} + \tau_\mu^{mem} \sqrt{\pi} \int_{x_\mu^{re}}^{x_\mu^{th}} du e^{u^2} (1 + \operatorname{erf}(u)) \right)^{-1}.$$

As before, we compute the step function derivatives, equation 3.15,

$$\begin{aligned} \partial_\lambda a_\mu(\{m_\gamma\}) &= -\frac{1}{T} \left(v_\mu^2 \tau_\mu^{mem} \sqrt{\pi} (e^{(x_\mu^{th})^2} (1 + \operatorname{erf}(x_\mu^{th})) \partial_\lambda x_\mu^{th} \right. \\ &\quad \left. - e^{(x_\mu^{re})^2} (1 + \operatorname{erf}(x_\mu^{re})) \partial_\lambda x_\mu^{re} \right) + \delta_{\lambda\mu} \\ \partial_\lambda \partial_\eta a_\mu(\{m_\gamma\}) &= \frac{2 \partial_\lambda v_\mu \partial_\eta v_\mu}{T v_\mu} - \frac{v_\mu^2 \tau_\mu^{mem} \sqrt{\pi}}{T} \\ &\quad \times \left(\left(2 x_\mu^{th} e^{(x_\mu^{th})^2} (1 + \operatorname{erf}(x_\mu^{th})) + \frac{2}{\sqrt{\pi}} \right) \partial_\lambda x_\mu^{th} \partial_\eta x_\mu^{th} \right. \\ &\quad \left. + e^{(x_\mu^{th})^2} (1 + \operatorname{erf}(x_\mu^{th})) \partial_\lambda \partial_\eta x_\mu^{th} \right. \\ &\quad \left. - \left(2 x_\mu^{re} e^{(x_\mu^{re})^2} (1 + \operatorname{erf}(x_\mu^{re})) + \frac{2}{\sqrt{\pi}} \right) \partial_\lambda x_\mu^{re} \partial_\eta x_\mu^{re} \right. \\ &\quad \left. - e^{(x_\mu^{re})^2} (1 + \operatorname{erf}(x_\mu^{re})) \partial_\lambda \partial_\eta x_\mu^{re} \right) \end{aligned}$$

with

$$\begin{aligned} \partial_\lambda x_\mu^{th/re} &= \frac{-Q_\mu^{th/re} \Psi_{\lambda\mu} - 4K_\mu \Phi_{\lambda\mu}}{4K_\mu^{3/2}} \\ \partial_\lambda \partial_\eta x_\mu^{th/re} &= \frac{4K_\mu (\Phi_{\lambda\mu} \Psi_{\eta\mu} + \Phi_{\eta\mu} \Psi_{\lambda\mu}) + 3Q_\mu^{th/re} \Psi_{\lambda\mu} \Psi_{\eta\mu}}{16K_\mu^{5/2}}. \end{aligned}$$

From now on, the current-based model can be used to perform a parameter space exploration. The stationary solutions can be numerically computed for any set of parameters and compared with network simulations. This is done in section 3.4.

3.3.3 Conductance-Based Models. For the conductance-based model, every synaptic event results in an increase in the corresponding conductance, and the integrate-and-fire equation can be written as

$$C_\mu^{mem} \frac{d}{dt} V_\mu(t) = G_\mu^L (V_\mu^{rest} - V_\mu(t)) + G_{\alpha\mu}(t) (E_\alpha - V_\mu(t)), \quad (3.42)$$

where C_μ^{mem} and G_μ^L are the membrane capacitance and leak conductance, respectively, such that $\frac{C_\mu^{mem}}{G_\mu^L} = \tau_\mu^{mem}$ is the resting membrane time constant. $G_{\alpha\mu}$ is the total conductance of the synaptic set α and E_α the corresponding reversal potential. Similar to the current-based model, the synaptic input can be modeled by Poisson processes, and the total conductance of the synapses α is

$$G_{\alpha\mu}(t) = \int_{\mathbb{R}} g_{\alpha\mu}(t-s) N_{\alpha\mu}(ds), \quad (3.43)$$

where $g_{\alpha\mu}(t)$ is the conductance time course elicited by an incoming spike from population α . We can write equation 3.42 in an analogous form to the current-based model with an effective membrane time constant $\tau_\mu^{eff}(t)$,

$$\tau_\mu^{eff}(t) \frac{d}{dt} V_\mu(t) = -V_\mu(t) + \frac{G_\mu^L V_\mu^{rest} + G_{\alpha\mu}(t) E_\alpha}{G_\mu^{tot}(t)}, \quad (3.44)$$

where the total conductance and the effective time constant are defined as follows:

$$G_\mu^{tot}(t) = G_\mu^L + \sum_{\alpha=1, \dots, K} G_{\alpha\mu}$$

$$\tau_\mu^{eff}(t) = \frac{C_\mu^{mem}}{G_\mu^{tot}(t)}.$$

Even when the synaptic input is considered as white noise, equation 3.42 cannot be solved, and there is no exact solution for the transfer function. We can use equation 3.27 as a first approximation, but we need to compute the mean membrane potential $\langle V_\mu \rangle$ and the variance $\sigma^2(V_\mu)$ in the conductance-based model. Equation 3.44 can be approximated by the following effective current-based equation (Kuhn, Aertsen, & Rotter, 2004),

$$\langle \tau_\mu^{eff} \rangle \frac{d}{dt} V_\mu(t) = -V_\mu(t) + \frac{G_\mu^L V_\mu^{rest} + \langle G_{\alpha\mu} \rangle E_\alpha}{\langle G_\mu^{tot} \rangle}, \quad (3.45)$$

with

$$\langle G_{\alpha\mu} \rangle = C_{\alpha\mu} (m_\alpha + m_\alpha^{ext}) \int_{\mathbb{R}} ds g_{\alpha\mu}(ds)$$

$$\langle G_\mu^{tot} \rangle = G_\mu^L + \sum_{\alpha=1, \dots, K} \langle G_{\alpha\mu} \rangle$$

$$\langle \tau_\mu^{eff} \rangle = \frac{C_\mu^{mem}}{\langle G_\mu^{tot} \rangle}$$

Synapse model. Following Kuhn et al. (2004), we can deduce from equation 3.45 a good approximation for the mean membrane potential and the variance. The mean membrane potential is given by the following form,

$$\langle V_\mu \rangle = \langle \tau_\mu^{eff} \rangle \left(\frac{V_\mu^{rest}}{\tau_\mu^{mem}} + \frac{E_\alpha}{C_\mu^{mem}} \langle G_{\alpha\mu} \rangle \right) \quad (3.46)$$

$$= \langle \tau_\mu^{eff} \rangle \left(\frac{V_\mu^{rest}}{\tau_\mu^{mem}} + \Phi_{\alpha\mu} (m_\alpha + m_\alpha^{ext}) \right), \quad (3.47)$$

where

$$\Phi_{\alpha\mu} = C_{\alpha\mu} \frac{E_\alpha}{C_\mu^{mem}} \int_{\mathbb{R}} ds g_{\alpha\mu}(ds)$$

depends on the chosen synapse. Using this mean membrane potential, equation 3.45 can be integrated for a synaptic event while the neuron is clamped around the mean value $\langle V_\mu \rangle$. The corresponding $PSP_{\alpha\mu}(t)$ allows us to compute the variance:

$$\sigma^2(V_\mu) = C_{\alpha\mu} (m_\alpha + m_\alpha^{ext}) \int_{\mathbb{R}} ds PSP_{\alpha\mu}^2(s) \quad (3.48)$$

$$= \frac{\Psi_{\alpha\mu}}{2} (m_\alpha + m_\alpha^{ext}). \quad (3.49)$$

We have to specify the form of $\Phi_{\alpha\mu}$ and $\Psi_{\alpha\mu}$ for different synapses. For the conductance-based model, we consider only exponential synapses and α -synapses. Following the same computation as in the current-based model, we can determine the desired functions,

$$\Phi_{\alpha\mu}^{Exp} = \frac{\tau_\alpha \Delta g_{\alpha\mu} C_{\alpha\mu} E_\alpha}{C_\mu^{mem}} \quad \Phi_{\alpha\mu}^{\alpha syn} = \frac{e \tau_\alpha \Delta g_{\alpha\mu} C_{\alpha\mu} E_\alpha}{C_\mu^{mem}} \quad (3.50)$$

and

$$\Psi_{\alpha\mu}^{Exp} = \frac{C_{\alpha\mu}}{\tau_\alpha + \langle \tau_\mu^{eff} \rangle} \left(\frac{\tau_\alpha \Delta g_{\alpha\mu} \langle \tau_\mu^{eff} \rangle (E_\alpha - \langle V_\mu \rangle)}{C_\mu^{mem}} \right)^2 \quad (3.51)$$

$$\Psi_{\alpha\mu}^{\alpha syn} = \frac{1}{2} C_{\alpha\mu} (2 \langle \tau_\mu^{eff} \rangle + \tau_\alpha) \left(\frac{e \tau_\alpha \Delta g_{\alpha\mu} \langle \tau_\mu^{eff} \rangle (E_\alpha - \langle V_\mu \rangle)}{C_\mu^{mem} (\tau_\alpha + \langle \tau_\mu^{eff} \rangle)} \right)^2, \quad (3.52)$$

where $\Delta g_{\alpha\mu}$ is the synaptic strength.

Neuron transfer function in the master equation. The main difference with the current-based model is that the effective time constant is now activity dependent, and $\Psi_{\alpha\mu}$ depends on the mean membrane potential. We consider

that the leading time constant in the neuron dynamic is the effective time constant whatever the regime. The corresponding approximated transfer function can be written as

$$\nu_\mu = \frac{1}{2\langle\tau_\mu^{eff}\rangle} \left(1 + erf\left(\frac{\langle V_\mu \rangle - V_\mu^{threshold}}{\sqrt{2}\sigma(V_\mu)}\right) \right). \quad (3.53)$$

The computation is thus more complicated but still straightforward. We first define as previously the functions

$$Q_\mu = \langle V_\mu \rangle - V_\mu^{threshold} \quad (3.54)$$

$$K_\mu = 2\sigma^2(V_\mu) \quad (3.55)$$

$$x_\mu = \frac{Q_\mu}{\sqrt{K_\mu}}. \quad (3.56)$$

Because those functions now depend on m_α in a more intricate way, the step function derivatives, equation 3.15, must be written as follows:

$$\begin{aligned} \partial_\lambda a_\mu(\{m_\gamma\}) = & \frac{1}{T} \left(\frac{e^{-x_\mu^2}}{\sqrt{\pi}\langle\tau_\mu^{eff}\rangle} \left(\frac{2K_\mu \partial_\lambda Q_\mu - Q_\mu \partial_\lambda K_\mu}{2K_\mu^{3/2}} \right) \right. \\ & \left. - \nu_\mu \frac{\partial_\lambda \langle\tau_\mu^{eff}\rangle}{\langle\tau_\mu^{eff}\rangle} - \delta_{\lambda\mu} \right), \end{aligned} \quad (3.57)$$

and for the second derivative,

$$\begin{aligned} \partial_\lambda \partial_\eta a_\mu(\{m_\gamma\}) = & \frac{e^{-x_\mu^2}}{\sqrt{\pi}T\langle\tau_\mu^{eff}\rangle} \left(\frac{1}{4K_\mu^{7/2}} \left(2K_\mu(2Q_\mu^2 - K_\mu)(\partial_\lambda Q_\mu \partial_\eta K_\mu + \partial_\eta Q_\mu \partial_\lambda K_\mu) \right. \right. \\ & + 4K_\mu^3 \partial_\eta \partial_\lambda Q_\mu - 8K_\mu^2 Q_\mu \partial_\lambda Q_\mu \partial_\eta Q_\mu \\ & \left. \left. + Q_\mu(3K_\mu - 2Q_\mu^2)\partial_\lambda K_\mu \partial_\eta K_\mu - 2K_\mu^2 Q_\mu \partial_\eta \partial_\lambda K_\mu \right) \right. \\ & - \left(\frac{2K_\mu \partial_\lambda Q_\mu - Q_\mu \partial_\lambda K_\mu}{2K_\mu^{3/2}} \right) \frac{\partial_\eta \langle\tau_\mu^{eff}\rangle}{\langle\tau_\mu^{eff}\rangle} \\ & - \left(\frac{2K_\mu \partial_\eta Q_\mu - Q_\mu \partial_\eta K_\mu}{2K_\mu^{3/2}} \right) \frac{\partial_\lambda \langle\tau_\mu^{eff}\rangle}{\langle\tau_\mu^{eff}\rangle} \\ & \left. + 2 \frac{\partial_\lambda \langle\tau_\mu^{eff}\rangle \partial_\eta \langle\tau_\mu^{eff}\rangle}{T\langle\tau_\mu^{eff}\rangle^2} - \frac{\partial_\lambda \partial_\eta \langle\tau_\mu^{eff}\rangle}{T\langle\tau_\mu^{eff}\rangle} \right), \end{aligned}$$

with

$$\begin{aligned} Q_\mu &= \langle \tau_\mu^{eff} \rangle \left(\frac{V_\mu^{rest}}{\tau_\mu^{mem}} + \Phi_{\alpha\mu}(m_\alpha + m_\alpha^{ext}) \right) - V_\mu^{threshold} \\ \partial_\lambda Q_\mu &= \partial_\lambda \langle \tau_\mu^{eff} \rangle \left(\frac{V_\mu^{rest}}{\tau_\mu^{mem}} + \Phi_{\alpha\mu}(m_\alpha + m_\alpha^{ext}) \right) + \langle \tau_\mu^{eff} \rangle \Phi_{\lambda\mu} \\ \partial_\eta \partial_\lambda Q_\mu &= \partial_\eta \partial_\lambda \langle \tau_\mu^{eff} \rangle \left(\frac{V_\mu^{rest}}{\tau_\mu^{mem}} + \Phi_{\alpha\mu}(m_\alpha + m_\alpha^{ext}) \right) + \partial_\eta \langle \tau_\mu^{eff} \rangle \Phi_{\lambda\mu} \\ &\quad + \partial_\lambda \langle \tau_\mu^{eff} \rangle \Phi_{\eta\mu} \end{aligned}$$

and

$$\begin{aligned} K_\mu &= \Psi_{\alpha\mu}(m_\alpha + m_\alpha^{ext}) \\ \partial_\lambda K_\mu &= \partial_\lambda \Psi_{\alpha\mu}(m_\alpha + m_\alpha^{ext}) + \Psi_{\lambda\mu} \\ \partial_\eta \partial_\lambda K_\mu &= \partial_\lambda \partial_\eta \Psi_{\alpha\mu}(m_\alpha + m_\alpha^{ext}) + \partial_\eta \Psi_{\lambda\mu} + \partial_\lambda \Psi_{\eta\mu}. \end{aligned}$$

The derivatives of functions $\langle \tau_\mu^{eff} \rangle$ and $\Psi_{\alpha\mu}$ are given in appendix C. The conductance-based model is now completely specified and can be used for a parameter space exploration as well.

3.4 Numerical Results. Simulations were done to compare the predicted stationary states given by the master equation and the corresponding neuron networks. In section 3.4.1, we explore different parameter spaces for the current-based neuron model, and the conductance-based neuron network is studied in section 3.4.2. Section 3.4.3 is devoted to more general models where a more realistic connectivity scheme is used.

3.4.1 Current-Based Models. We consider here two types of state diagrams based on the literature. The three concerned parameters are the external excitatory firing rate stimulation m_{exc}^{ext} and the excitatory/inhibitory synaptic strength A_μ with $\mu \in \{exc, inh\}$. With those parameters, we were interested in the (m_{exc}^{ext}, g) space where $g = \frac{A_{inh}}{A_{exc}}$, as in Brunel (2000) and Mehring et al. (2003). The second type of state diagram is generated by varying independently the excitatory and inhibitory synaptic strength (A_{exc}, A_{inh}) by feeding the network with a constant current in every neuron to sustain the activity (Vogels & Abbott, 2005). For each simulation, we want to investigate whether the model can provide a good prediction for the first and second statistical moments. Therefore, we systematically compare the mean activity and the standard deviation. First-order predictions have already been studied for similar network models (Brunel, 2000), and the corrective term

due to the second-order development does not contribute much. However, because we suggest using another neuron transfer function in the following, it is still interesting to perform the first-order analysis. For those simulations, $N = 5000$ neurons with a probability connection $p^{conn} = 0.01$. Neurons' intrinsic properties are homogeneous, with a membrane time constant $\tau_{\mu}^{mem} = 20$ ms, a refractory period $\tau_{\mu}^{ref} = 5$ ms, the resting potential and the reset potential $V_{\mu}^{rest} = V_{\mu}^{reset} = -60$ mV, the threshold potential $V_{\mu}^{threshold} = -50$ mV, and the membrane resistance $R_{\mu}^{mem} = 100$ M Ω for $\mu \in \{exc, inh\}$. Synaptic properties and external stimulations depend on the parameter space under consideration.

The (m_{exc}^{ext}, g) parameter space. For this state diagram we took exponential synapses with $\tau_{exc} = 1$ ms and $\tau_{inh} = 3$ ms for the excitatory and inhibitory synaptic time constants. The external stimulation will be considered in the v_{th} unit which is the frequency needed to bring the mean membrane potential to threshold with an excitatory Poisson input. As we are using exponential synapses we have, based on equation 3.34,

$$v_{th} = \frac{V^{threshold} - V^{rest}}{J_{exc} C_{exc} \tau_{exc}},$$

where $J_{exc} = R^{mem} A_{exc}$, we have omitted the second index because of network homogeneity. We chose $A_{exc} = 0.02$ pA such that the resulting EPSP peak is $J_{exc} = 2$ mV. The inhibitory synaptic strength is defined by $A_{inh} = g A_{exc}$ where g is the second parameter. We represent in Figure 2a the network mean cross-correlation and interspike interval to characterize the asynchronous irregular states.

Three regions can be outlined: a broad AI domain, an intermediate asynchronous regular (AR) region where neurons begin to fire periodically, and saturated synchronous regular (SR) states. We were interested in the AI regime in which the Markovian approximation is assumed to apply. Therefore, we limited our analysis of the parameter regime to firing rates below $1/\tau^{mem} = 50$ Hz. Above this frequency, long-range correlations in each neuron firing appear, and the analytical framework is not well suited to predict the macroscopic quantities. This is manifest by the emergence of a new peak near 0 in the ISI CV distribution (not shown), whereas interneuron correlations reach very small values. The absence of synchronous irregular states (SI) for high firing rates is essentially due to the absence of interaction delays between the neurons (Brunel, 2000). When a finite homogeneous delay is present, SI states could occur in the transitory region (Mehring et al., 2003); however, if the delays are drawn randomly from a broad distribution, this SI transition region is replaced by AR states. In the low-activity region, there is an increase of synchrony concomitant with a decrease in the mean ISI CV typical of slow SI states. For the whole region, as long as the network

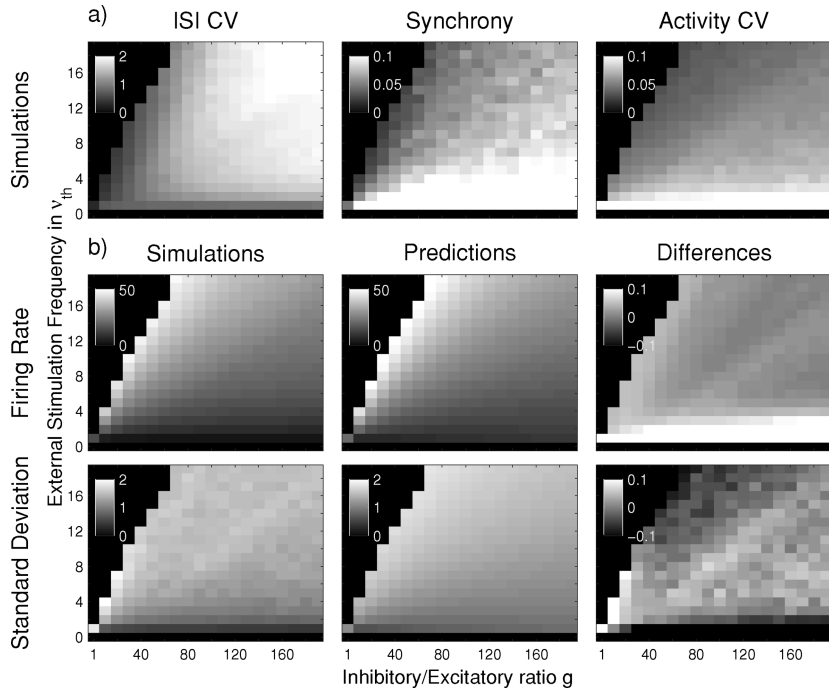


Figure 2: Characterization of the AI states and the first- and second-order statistics of the excitatory population activity in the (m_{exc}^{ext}, g) parameter space, similar to Brunel (2000). The network contains $N = 5000$ neurons randomly connected with probability $p^{conn} = 0.01$ and current-based synaptic interactions. Every statistical quantity has been computed with a time bin of $T = 5$ ms, and the analytical model was solved with the same parameters. (a) The AI region is delimited using the mean ISI CV and the mean pairwise cross-correlation. In the right panel, we compute the activity CV to evaluate the validity of the independence hypothesis. (b) Top: Mean activity estimated from numerical simulations (left) and computed using the master equation formalism (middle). In the right panel, the relative difference between measured and predicted values. Bottom: The activity standard deviation is estimated from numerical simulations and compared as well with the mean-field predictions.

is homogeneous and the neuron are independents, the synchrony phase diagram should be well predicted by the activity second-order statistics. More precisely, it should be directly related to the activity coefficient of variation (CV). Therefore, in the last panel in (see Figure 2a), we computed the activity CV, which can be compared with the synchrony panel. Both diagram exhibit the same tendency according to the parameter regime. Thus, this quantity could be estimated in the framework of the independence

hypothesis as long as the first- and second-order statistics are well predicted.

In Figure 2b, we computed and compared the mean excitatory activity and the standard deviation of excitatory activity for the parameter space. For each point, a simulation was run for 10 s in order to have an acceptable evaluation of the second-order statistics. The corresponding stationary quantities were numerically computed using the master equation formalism, equation 3.16, with the transfer function, equation 3.29. To compare our prediction with simulations, we computed the relative difference,

$$\Delta(m_{exc}^{ext}, g) = \frac{O_{Simulation}(m_{exc}^{ext}, g) - O_{Prediction}(m_{exc}^{ext}, g)}{|O_{Simulation}(m_{exc}^{ext}, g)| + |O_{Prediction}(m_{exc}^{ext}, g)|},$$

where O can be either the mean activity or the standard deviation. First-order and second-order statistics are in good agreement over almost the entire AI region with a relative error smaller than 0.1. However, the relative error is larger in the low-activity regime, as can be seen in Figure 2b. The reasons are twofold. On the one hand, for small networks exhibiting low activity, the synaptic input impinging on each neuron is equally low, and the diffusion approximation at the membrane potential level is not a good approximation anymore. On the other hand, the increase of pairwise correlations among neurons could partially invalidate the model, as can be seen from the discrepancies between the synchrony and the activity CV. For very large networks, a mean-field approach can be recovered even in the low-activity regime, and it provides accurate predictions (Kumar et al., 2008).

As the *in vivo* activity in awake animals usually displays low firing rates, we further investigated whether larger networks could generate more realistic cortical activity regimes. In Figure 3a, we show the results of a simulation of a larger network ($N = 15,000$ neurons) while keeping other parameters exactly the same as used in the simulation of a smaller network described in Figure 2. It is apparent that the region between 6 Hz and 10 Hz, which was not well predicted previously, can now be better described by the mean-field approach (with relative errors smaller than 0.1). This region is delimited by black curves in Figure 3a.

To pursue this analysis, we chose a row of parameters in the phase diagram and computed the mean firing rate numerically and with the master equation for various network sizes. We found that the relative error for each network size increased very slightly for smaller firing rates, as expected (see Figure 3b). However, the relative error still stays below 0.1, even for firing rates around 5 Hz. The corresponding predicted firing rates are given in Figure 3c for the different network sizes. The error bars are computed with the relative error using $O_{Prediction}(m_{exc}^{ext}, g) |\Delta(m_{exc}^{ext}, g)|$. In the right panel, we show for a particular point of the phase diagram $(m_{exc}^{ext}, g) = (6 \cdot v_{th}, 141)$ a decrease in firing rate as well as an increase in the relative error. The

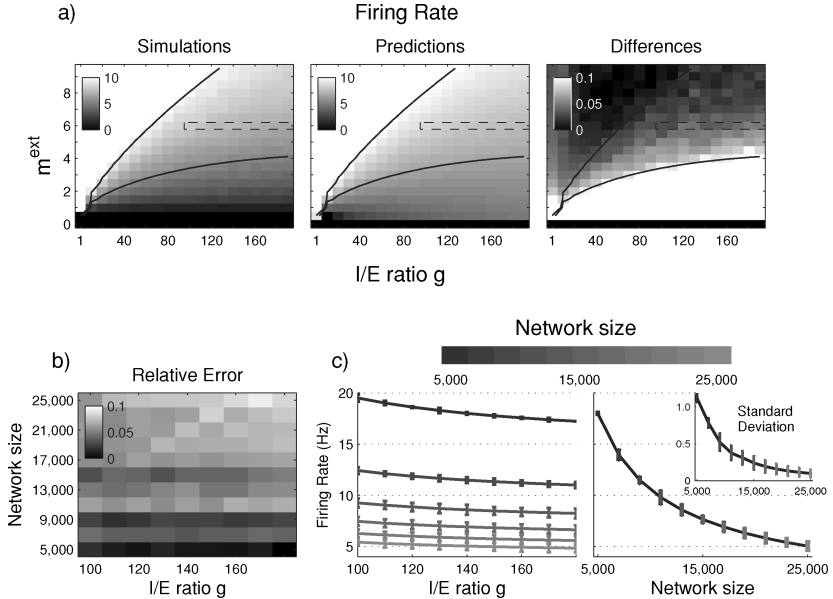


Figure 3: Master equation predictions for low firing rates depend on network size. (a) A large network of $N = 15,000$ neurons has been used to draw a similar phase diagram as in Figure 2. The region between the two black curves exhibits firing rates smaller than 10 Hz (higher curve) and relative errors smaller than 0.1 (lower curve). The predictions are improved for a broad range of frequencies compared to a smaller network. (b) The relative error between numerical simulations and predictions for a row of parameters in the phase diagram (indicated by a dashed rectangle in *a*) for different network sizes. (c) The relative error is slightly increasing for larger networks, but the firing rate decreases at the same time. Left: Predicted firing rate in the row for each network size. The error bars indicate the relative error in units of the corresponding predicted value. The firing rates decrease quickly compared to the error. Right: The firing rate decreases as a function of network size, for a particular point in the phase diagram ($m_{ext}^{ext}, g = (6 \cdot v_{th}, 141)$). Inset: Decay of the standard deviation with the network size. All networks had identical parameters as in Figure 2.

predicted firing rate seems to decrease exponentially compared to the relative error, which does not change much. A similar tendency has been found for the standard deviation. The inset of the right panel of Figure 3c shows that the error remains almost constant while the activity standard deviation decreases for larger networks. The activity coefficient of variation indicates that the averaged pairwise correlations also decrease. Therefore, based on this result, it should be possible to find large enough networks to cover a realistic range of firing frequencies.

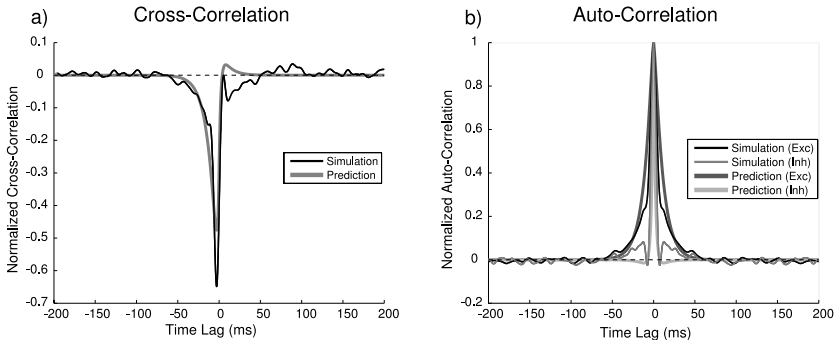


Figure 4: Correlation functions for the specific point $(m_{exc}^{ext}, g) = (8 \cdot v_{th}, 41)$ of Figure 2. (a) Cross-correlation between inhibitory and excitatory population activity for the master equation (thick line) and the numerical simulations (thin line). (b) Autocorrelation functions computed from the master equation for the inhibitory and excitatory activity (thick lines) and with $T = 10$ ms. The same functions have been estimated from the numerical simulations (thin lines). The activity traces have been computed with a bin size of 1 ms and then filtered with a gaussian function to get a smoother curve. The gaussian standard deviation was chosen to be $1.5T$ to match the corresponding function without filtering.

Covariance and inhibitory population statistics are equally well predicted. To compare the activity correlations, we chose a point in the parameter space for which we estimated the inhibitory and excitatory autocorrelation and the cross-correlation. The corresponding functions were computed from the master equation using the last equation of equation 3.16 and the stationary mean activity computed for that particular state (see Figure 4). To keep a good resolution of the numerical functions, we took a time bin $T = 10$ ms and filter the signal with a gaussian function with a standard deviation equal to $1.5T$. This gives a good prediction except for some part of the function, which can be due to a temporal finite-size effect. Indeed, the network is homogeneous, so the only difference between both populations is the size. If those populations are not large enough, residual oscillations that could not be predicted in our framework occur in the correlation functions. These oscillations also appear when the bin size T is too small (see Figure 1b). According to equation 3.16, we know that the interplay between network size and the considered timescale must be carefully taken into account to validate the model. For a very large network size or time constant T , the fast oscillations completely vanish. Moreover, we know from equation 3.16 that the correlation matrix depends directly on the neuron transfer function first derivative. More precisely, the predicted correlation exponential decrease as well as the activity standard deviation are led by this function. Therefore, regions where the autocorrelation and

the cross-correlation functions can be correctly described are regions where the second-order statistics match the numerical simulations.

The (A_{exc}, A_{inh}) parameter space. To reproduce results obtained in Vogels and Abbott (2005), we chose a similar model to probe the (A_{exc}, A_{inh}) parameter space. In the AI regime, current-based neurons cannot sustain activity without external stimulation, and one needs to inject a constant input in each neuron by bringing the resting potential to $V^{rest} = -49$ mV, as in the original letter. We also took exponential synapses with excitatory and inhibitory time constant $\tau_{exc} = 5$ ms and $\tau_{inh} = 10$ ms, respectively. The only free parameters remaining are the current quantal increments (A_{exc}, A_{inh}). We first computed the mean ISI CV, the mean pairwise cross-correlation, and the activity CV to find the boundaries of the AI region. As in the previous section, the state diagram was drawn in the AI regime for the excitatory population with the master equation prediction using equation 3.29 and the neuron network simulations (see Figure 5). The mean activity prediction is in good agreement with the numerical simulations, with a relative error smaller than 0.1, as shown in the first row of Figure 5b. The relative error is larger for the low-activity regime (<8 Hz), where it can reach 0.2. This can be understood as previously; in this region, the synaptic input is not strong enough to fulfill the required conditions for the diffusion approximation. This error can be reduced for larger networks (see Figure 3). The prediction for the standard deviation matches quite well except for the region of high and low activity, where the difference is more substantial. The latter can be expected from the first-order comparison. Concerning the former, the region is at the boundary of the AR regime, and the Markov hypothesis begins to fail because of the emergence of regularities in the neuron individual firing.

Similar simulations were done using the transfer function, equation 3.28, and the resulting predictions were worse compared to previous results (not shown). This transfer function has been obtained as a first-order approximation for exponential synaptic noise when the ratio $\sqrt{\frac{\tau_{syn}}{\tau_{mem}}}$ is small. In the numerical simulations here, the inhibitory synaptic time constant is only half the membrane time constant, and the assumption underlying equation 3.28 begins to fail. The phenomenological transfer function, equation 3.29, therefore seems more appropriate for these neuron properties.

3.4.2 Conductance-Based Models. Conductance-based neuron networks have been shown to display self-sustained activity for specific parameter space (Vogels & Abbott, 2005). For the $(\Delta g_{exc}, \Delta g_{inh})$ parameter space, two regions have been identified exhibiting, respectively, AI and SR states (see Figures 6a–6c).

In this section, we study a similar model with the resting membrane time constant $\tau^{mem} = 20$ ms, the membrane resistance $R^{mem} = 100$ M Ω , the

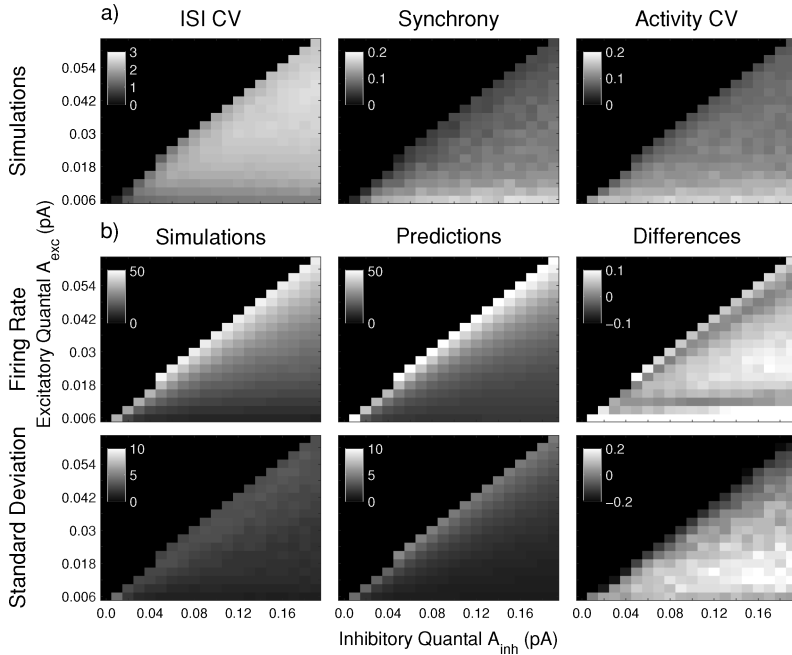


Figure 5: Characterization of AI states and the first- and second-order statistics of the excitatory population activity in the (A_{exc}, A_{inh}) parameter space, in a Vogels-Abbott-type current-based network. The network contains $N = 5000$ neurons randomly connected with probability $p^{conn} = 0.01$. Every statistical quantity has been computed with a time bin of $T = 5$ ms, and the analytical model was solved with the same parameters. (a) The AI region is delimited using the mean ISI CV and the mean pairwise cross-correlation. In the right panel, we compute the activity CV to evaluate the validity of the independence hypothesis. (b) Top: Mean activity estimated from numerical simulations (left) and computed using the master equation formalism (middle). In the right panel, the relative difference between measured and predicted values. Bottom: The activity standard deviation is estimated from numerical simulations and compared as well with the mean-field predictions.

resting and reset membrane potential $V^{rest} = V^{reset} = -60$ mV, the threshold $V^{threshold} = -50$ mV, and the refractory period $\tau^{ref} = 5$ ms. Synaptic time constant and reversal potential are taken to be $\tau_{exc} = 5$ ms, $E_{exc} = 0$ mV, $\tau_{inh} = 10$ ms, and $E_{inh} = -80$ mV for excitatory and inhibitory synapses, respectively. Given the state diagram (see Figures 6a–6c), we see that the AI region is surrounded by unstable states, which is not present in the current-based correspondent (compare with Figure 5). This is a specificity of the conductance-based model and an interesting issue that should be discussed

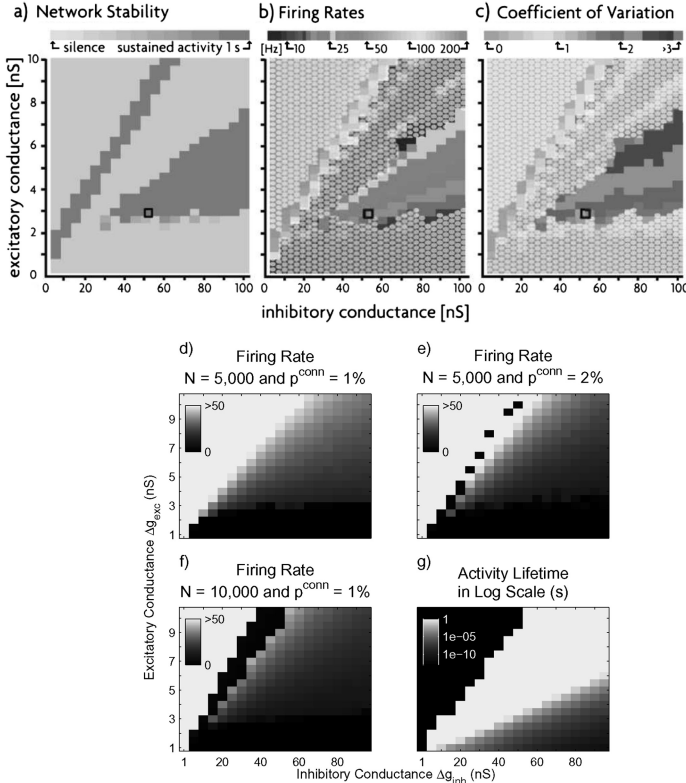


Figure 6: Sources of instabilities in Vogels-Abbott-type networks. Study of the stability (a), the mean activity (b), and the mean ISI CV (c) in the $(\Delta g_{exc}, \Delta g_{inh})$ parameter space for a self-sustained conductance-based neuron network. The network in panels a to c contains $N = 10,000$ neurons, each randomly connected with $p^{conn} = 0.02$ of the population. The network is considered stable if its activity lasts longer than 1 s. (a–c modified, with authorization, from Vogels and Abbott, 2005). (d–f) Excitatory population mean activity for different network structures. For these numerical simulations, the network is considered stable if its activity lasts longer than 3 s. The transitory region between the AI and the SR domain in the $(\Delta g_{exc}, \Delta g_{inh})$ parameter space is sensitive to synaptic input fluctuation. (d) Network of $N = 5000$ neurons with $p^{conn} = 0.01$. The AR domain is fully stable. (e) Network of $N = 5000$ neurons with $p^{conn} = 0.02$. Some disparate points in the AR domain lose their stability. (f) Network of $N = 10,000$ neurons with $p^{conn} = 0.01$. The AR domain is almost completely unstable. (g) Network lifetime in log scale computed in the $(\Delta g_{exc}, \Delta g_{inh})$ parameter space for a network of $N = 10,000$ neurons and $p^{conn} = 0.01$. We took $m_{crit} = 1$ Hz for the critical activity because no self-sustained activity of 1 Hz could be produced with this network model. Furthermore, this prediction has been computed by using the effective transfer function introduced below. Stability criteria match qualitatively with f for the low-activity AI region.

about the network stability in numerical simulation and the corresponding master equation prediction.

Stability in self-sustained networks. According to the stationary solution of the master equation, the active state could be unstable or stable in the usual sense. However, for stable points, there is an important consideration to take into account to match the numerical simulations. The framework presented here is a mean-field solution that does not take into account every finite-size effect that can be encountered in numerical models. For instance, stable states in the model with very weak activity are not sustained in network simulation. In some cases, the network activity fluctuations are too strong and can bring the dynamics to a quiescent state after a transient period. It has been shown that for multi-unit systems such as neural networks, a quasi-stationary state could survive for a period that is exponentially proportional to the system size (Crutchfield & Kaneko, 1988). More particularly, in self-sustained conductance-based networks, the state loses its stability when the network activity exhibits fluctuations that are too strong (Kumar et al., 2008). Therefore, we can adopt a criterion to keep those states with large fluctuations according to the timescale we are interested in. For instance, in Vogels and Abbott (2005), a network is said to be stable if it can sustain its activity longer than a second. Those networks will eventually fall into a quiescent state after a long transient. In our framework, once the equations are solved, we can compute the total mean activity and the total variance. For a balanced network, we have

$$\begin{aligned}\langle m_{tot} \rangle &= \langle (1 - \gamma)m_{exc} + \gamma m_{inh} \rangle \\ &= (1 - \gamma)\langle m_{exc} \rangle + \gamma \langle m_{inh} \rangle \\ \sigma^2(m_{tot}) &= \langle ((1 - \gamma)m_{exc} + \gamma m_{inh})^2 \rangle - \langle (1 - \gamma)m_{exc} + \gamma m_{inh} \rangle^2 \\ &= (1 - \gamma)^2\sigma^2(m_{exc}) + \gamma^2\sigma^2(m_{inh}) + 2(1 - \gamma)\gamma c_{exc/inh}.\end{aligned}$$

As m_{exc} and m_{inh} are described as a normal law defined by only the first two statistical moments, the total activity also follows a normal law with the following characteristics:

$$\begin{aligned}m_{tot} &\sim \mathcal{N}((1 - \gamma)\langle m_{exc} \rangle + \gamma \langle m_{inh} \rangle, (1 - \gamma)^2\sigma^2(m_{exc}) \\ &\quad + \gamma^2\sigma^2(m_{inh}) + 2(1 - \gamma)\gamma c_{exc/inh}).\end{aligned}\tag{3.58}$$

Therefore, we can use a simple criterion for stability by saying that the survival time is inversely proportional to the probability for the activity to be below a critical value m_{crit} near 0. Indeed, the spontaneous AI state is said to be quasi-stationary such that its activity is described by a stationary distribution. Eventually the dynamics will fall into this quiescent state, which is represented in mean-field theory by the probability below m_{crit}

normalized by the minimal time step,

$$T_{survival} = \frac{T}{P(m_{tot} < m_{crit})} \quad (3.59)$$

$$= \frac{T}{F(m_{tot} = m_{crit})}, \quad (3.60)$$

where $F(m_{tot} = m)$ is the repartition function. A similar criterion has been proposed in Kumar et al. (2008) but based on a first-order semianalytical model. In their argument, they mention a critical time window that corresponds to our network effective time constant T . In numerical simulations, they could estimate its value around 1 ms, which is very short compared to other time constants in the network model. This is encouraging for considering the master equation formalism well beyond large time constants. We can easily see from equations 3.16 and 3.22 that the covariance matrix is inversely proportional to the number of neurons in each population, so that $T_{survival}$ grows exponentially with the number of neurons. Discrepancy from this result can be caused by residual correlations between neurons that could invalidate the binomial model. We can further estimate the network lifetime dependency on other parameters. We show in Figure 6g in a log scale the network lifetime evaluated with equation 3.59 for the $(\Delta g_{exc}, \Delta g_{inh})$ parameter space for a network of $N = 10,000$ neurons with $p^{conn} = 0.01$. We see that the AI region considered unstable in Figure 6f matches the region where the lifetime is beyond the order of a second. Therefore, the state diagram for self-sustained networks is sensitive to the time-scale under consideration.

Despite the stability issue, which is due to the limited lifetime of the network activity, there is finally an important source of instability that can also cause the network to reach the quiescent state. We can see numerically in Figures 6d to 6f that if the subthreshold membrane potential fluctuations are too strong, this induces supplementary fluctuations at the network level, which can destroy the activity spontaneously. These strong fluctuations can be caused by high levels of connectivity. Therefore, the upper AI region, which is predicted to be stable, can be numerically unstable because of those strong fluctuations. In Kumar et al. (2008), this region is not systematically unstable, and the lack of evidence with a second-order theory seems to reveal an artifact of the simulation or the breakdown of the model prediction. The sensitive region lay between the AI and the SR regime in which correlations can become critical. Indeed, the AR region displays correlated spike trains, which is not taken into account within the Poisson hypothesis, and this could go beyond the Markovian prediction. Kumar et al. (2008), have also suggested that the initial stimulation could contribute to this instability. Indeed, the initial stimulation must be adequate to allow the network to reach a self-sustained state. Increasing the network size will diminish the

firing rate, as predicted by the numerical and analytical transfer function, making the network more likely to shut down given the fluctuation state. This instability is reduced for sparser connectivities.

The $(\Delta g_{exc}, \Delta g_{inh})$ parameter space. We focus on the last configuration shown in Figure 6 to check the validity of the theoretical prediction. For each stable point of the state diagram, the set of differential equation 3.16, is solved with the transfer function, equation 3.53. The resulting analysis (see Figure 7) shows that the predictions are qualitatively correct, but the relative difference increases rapidly for low activity. There is a narrow region in the AI regime where the prediction is good for the first and second statistical moments. This important discrepancy is due to the approximation made for the transfer function, which is not derived for a complete conductance-based neuron with threshold. Similar results have already been reported in Kuhn et al. (2004) using the same transfer function.

To circumvent this problem, a semianalytical method has been proposed (Soula & Chow, 2007; Kumar et al., 2008), where the conductance-based neuron transfer function is determined numerically and then used directly in the model for a first-order or second-order prediction. Although this approach can give good predictions in the AI regime, it requires computing numerically the transfer function for each point of the state diagram, which can be time-consuming for heterogeneous networks. Indeed, the transfer function is determined by computing the neuron firing rate for a given population and for every state of each population in the network. Therefore, it is necessary to find an effective analytical function that can provide a better approximation. Although we cannot have an exact expression, it is still possible to fit a phenomenological model to the numerical simulations. Based on previous observations, two parameters seem critical in the transfer function: the time constant τ in the denominator and a corrective term Δh , which takes into account colored noise in the synaptic input (Brunel & Sergi, 1998; Fourcaud & Brunel, 2002). The phenomenological function based on equation 3.27 can thus be written

$$\nu = \frac{1}{2\tau} \left(1 + erf \left(\frac{\langle V \rangle - V^{threshold}}{\sqrt{2}\sigma(V)} + \Delta h \right) \right). \quad (3.61)$$

Considering the limited region of the whole $(\Delta g_{exc}, \Delta g_{inh})$ parameter space in Figure 7, we can estimate the total error made for the set of transfer function, equation 3.61, according to the free parameters ($\tau, \Delta h$). The total error is estimated by taking the sum of the relative difference between the simulation mean activity and the mean activity given by equation 3.61 in absolute value normalized by the number of stable points. For this optimization problem, there is a global minimum for which the error is small (see Figure 8). This computation depends on the network configuration and

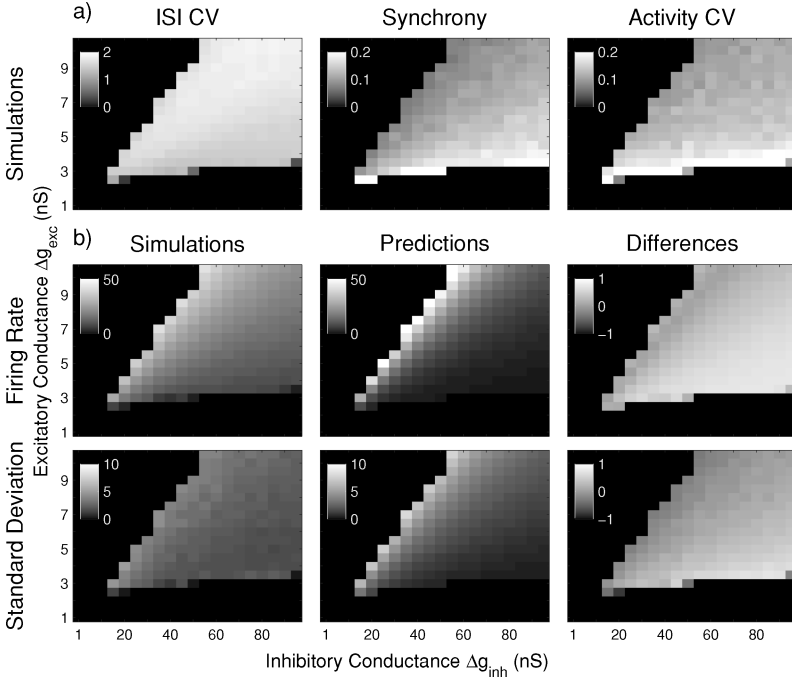


Figure 7: AI states characterization and the first- and second-order statistics of the excitatory population activity in the $(\Delta g_{exc}, \Delta g_{inh})$ parameter space in a Vogels-Abbott-type conductance-based network. The network contains $N = 10,000$ neurons randomly connected with probability $p^{com} = 0.01$. Every statistical quantity has been computed with a time bin of $T = 5$ ms, and the analytical model was solved with the same parameters. (a) The AI region is delimited using the mean ISI CV and the mean pairwise cross-correlation. In the right panel, we compute the activity CV to evaluate the validity of the independence hypothesis. (b) Top: Mean activity estimated from numerical simulations (left) and computed using the master equation formalism with the neuron transfer function, equation 3.53 (middle). In the right panel, the relative difference between measured and predicted values. Bottom: The activity standard deviation is estimated from numerical simulations and compared as well with the mean-field predictions.

the portion of the state diagram used to estimate the error. Therefore, this procedure gives a local good approximation that is acceptable as long as the network parameters (here the synaptic strengths) are kept in the fitted region.

The second-order statistics depends on the transfer function behavior around the stationary point through the first and second derivative of this

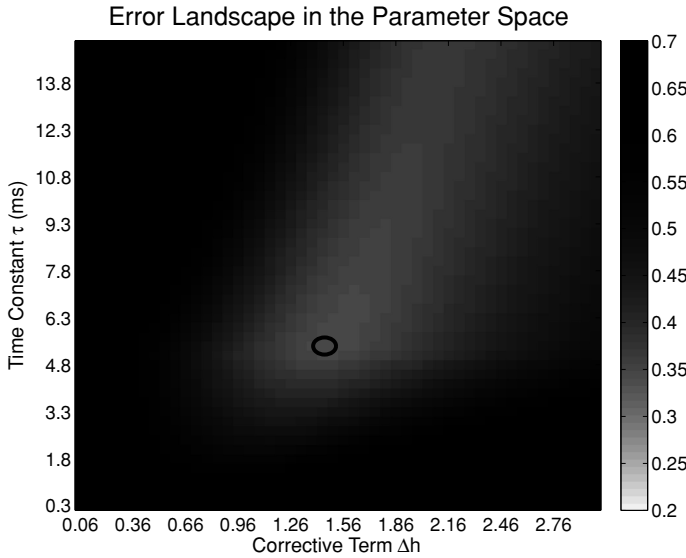


Figure 8: Error landscape for the optimization problem that determines the best parameter set for the effective transfer function, equation 3.61. It has been computed for a network of $N = 10,000$ neurons and $p^{conn} = 0.01$. The minimal solution (circle) gives $\tau = 5.3$ ms and $\Delta h = 1.5$.

function. In particular, the covariance and correlation matrix are strongly affected by the slope of the transfer function in the stationary point. Therefore, we compare for some point of the parameter space the effective transfer function with the semianalytical approach (see Figure 9). For each network configuration, the transfer function of a neuron is computed numerically and compared with the optimized transfer function. The local behavior around the stationary point is in good agreement with the latter.

Using the optimized transfer function, we can compare the prediction to the numerical simulation (see Figure 10). The error is reasonable compared to Figure 7, especially for the standard deviation for which prediction is much improved. Therefore, for a given network configuration, there is an effective transfer function that can provide a good description of the network dynamics in a large part of the parameter space. This allows us to avoid the semianalytical approach but requires solving an optimization problem based on numerical simulations.

This method could be useful when considering several network units described by the master equation. Indeed, eventually we would like to apply the master equation formalism to large-scale cortical recordings. In order to do so, it will be necessary to acquire a more realistic transfer function than

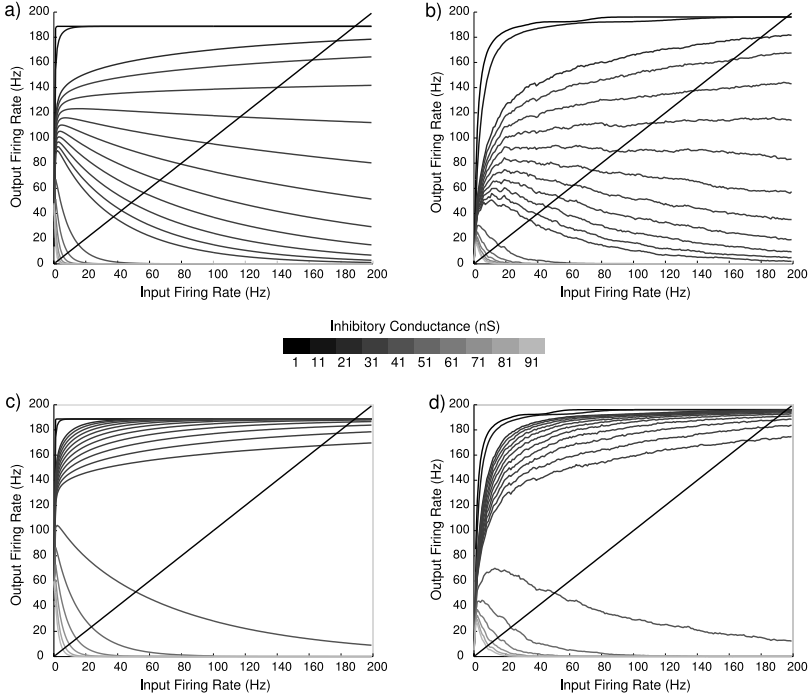


Figure 9: Transfer function estimated with the semianalytical approach compared with the optimized effective transfer function for several points of the $(\Delta g_{exc}, \Delta g_{inh})$ parameter space. For each figure, the excitatory synaptic strength is fixed, and the inhibitory synaptic strength take the values $\Delta g_{inh} = 1, 11, 21, 22, 23, 24, 25, 26, 27, 28, 29, 30, 31, 41, 51, 61, 71, 81$, and 91 nS from the top-most curve to the lowest monotonically. In the first-order mean-field approximation, the network stationary activity is found by imposing that the input and output rate must be equal. The intersection with the diagonal line marks this first-order solution. (a) Effective transfer function and (b) numerical transfer function for $\Delta g_{exc} = 7 \text{ nS}$. (c) Effective transfer function and (d) numerical transfer function for $\Delta g_{exc} = 10 \text{ nS}$.

the one obtained from integrate-and-fire neurons. Using the optimization strategy, we could consider a large family of functions based on the usual theoretical results and obtain a representative transfer function adapted to high-conductance states. This could be done with dynamic-clamp *in vitro* experiments by finding autoconsistent solutions for a broad range of stimulation regimes. The resulting transfer function would then be used as a kernel in the master equation formalism to represent the dynamical property of the corresponding neuron population in the network unit. In

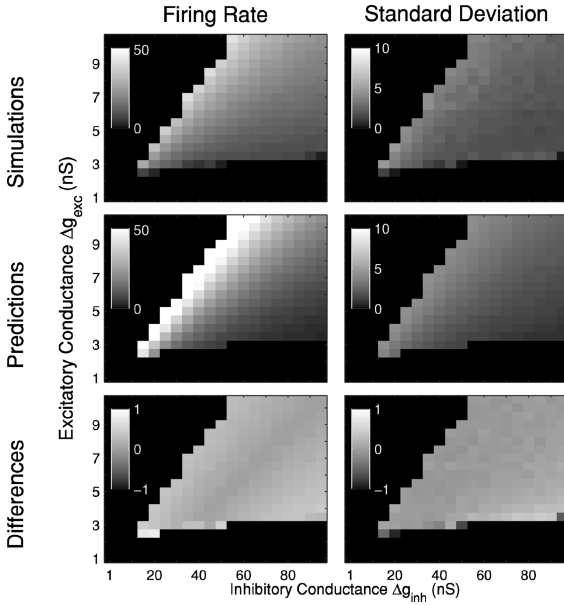


Figure 10: First- and second-order statistics of the excitatory population activity in the $(\Delta g_{exc}, \Delta g_{inh})$ parameter space. A Vogels-Abbott network was simulated with $N = 10,000$ conductance-based neurons randomly connected with probability $p^{conn} = 0.01$. The moments are computed with a time bin of $T = 5$ ms, and the analytical model was solved with the same parameter and an effective transfer function (see equation 3.61). (Top) Mean activity and standard deviation estimated from numerical simulations. (Middle) Mean activity and standard deviation computed from the master equation formalism. (Bottom) Relative difference between measured and predicted values.

the context of voltage-sensitive dyes optical imaging, this unit would be associated with a small set of neighbor pixels. Once effective couplings between these units are extracted from data, it should be possible to obtain a theoretical comparative model in order to study activity propagation within large-scale cortical areas, in particular, dynamical phase transitions according to different network-controlled conditions.

3.4.3 Effect of Topology and Heterogeneity. In this section, we discuss the generality of the master equation formalism and possible sources of deviations from the predictions. Heterogeneity in the synaptic input across the network can create a bias in the mean activity of the network that is not taken into account in a mean-field model. Indeed, if neurons in the network do not receive exactly the same number of synapses, the firing rate distribution in the network will tend to be skewed compared to the sharp gaussian

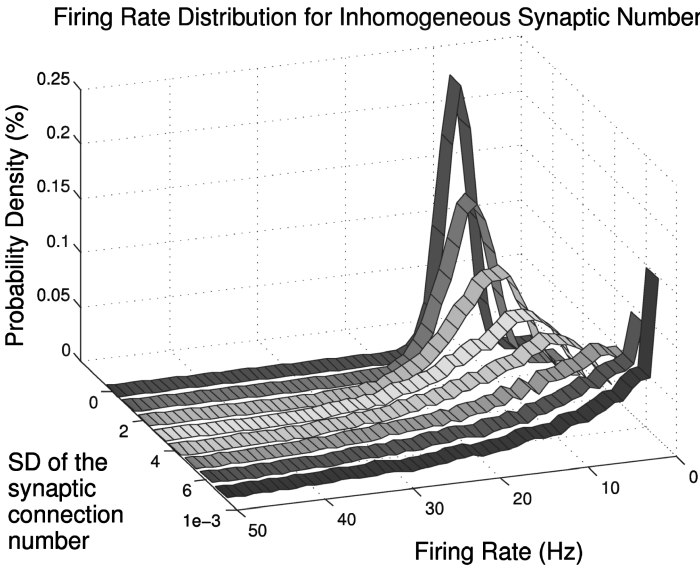


Figure 11: The neuron firing rate distribution in the AI state according to the degree of heterogeneity in the number of incoming synapses per neuron. The network contains $N = 10,000$ neurons with a mean connectivity proportion $p^{conn} = 0.02$. The synaptic strengths are given by $(\Delta g_{exc}, \Delta g_{inh}) = (6, 67)$ nS. The number of incoming synapses is taken from a gaussian distribution. From the back curve to the front curve, the standard deviation is increasing, resulting in skewer curves.

distribution for a homogeneous system. If the incoming connection number is gaussian distributed, the skewness of the firing rate distribution will increase with the standard deviation of the gaussian (see Figure 11), resulting in a shift of the mean activity. Similar results were reported by van Vreeswijk and Sompolinsky (1998) for heterogeneous thresholds. Therefore, predictions given by the master equation could lose some accuracy if the network is not perfectly homogeneous. However, this kind of heterogeneity does not create dramatic changes in the mean firing rate, so the model still provides good predictions.

Another interesting aspect of the theory concerns the connectivity schemes of the network. When the theoretical framework was built, two important hypotheses were made that directly concern network circuitry. We assumed that the connectivity is sparse and that the spiking probability is independent from one neuron to another at each time step. Any connectivity scheme that can account for those two hypotheses should be describable by this master equation formalism. Although connections in the cortex are highly specific, they are known to exhibit the sparseness property. As

we are describing macroscopic quantities of the network dynamics, high-order structure in the connectivity should not affect the analytical validity. However, the independence hypothesis can be broken if substantial correlations appear between neurons. In our simulations, we used a random connectivity scheme to avoid this situation. This choice is reasonable for very small networks, but for larger networks, it is necessary to consider a more realistic connectivity scheme. In previous work (Mehring et al., 2003), a numerical study of the (m_{exc}^{ext}, g) parameter space has been made for networks of locally random connected neurons with periodic boundary conditions. In this model, each neuron was connected to a fixed proportion $p^{conn} = 0.1$ of its neighbors according to a gaussian probability law (see Figure 12c). The standard deviation is taken to be 0.3 mm for a square network with boundary length of 2 mm. This network contains $N = 112,500$ current-based neurons with a ratio of 4:1 between excitatory and inhibitory neurons. Neurons interact with a fixed delay of 1.5 ms. The network is homogeneous with membrane time constant $\tau^{mem} = 10$ ms, refractory period $\tau^{ref} = 2$ ms, resting and reset potential $V^{reset} = V^{rest} = -70$ mV, and threshold $V^{threshold} = -50$ mV. α -synapses were used with $\tau_{exc} = \tau_{inh} = 0.3$ ms, and the excitatory synaptic strength was chosen such that the EPSP peak equals 0.14 mV. We implemented the same network in the formalism with the transfer function (see equation 3.29) and computed the excitatory mean activity to compare with their results (see Figures 12a and 12b). For this macroscopic quantity, it seems that correlations due to local connections do not dramatically alter the first-order mean-field predictions. This is very encouraging, and we hope to get qualitatively good descriptions of large-scale cortical networks based on this generic behavior of balanced networks. Of course, those who are interested in higher-order statistics of the dynamics have to rely on a more specific model of the network connectivity.

We investigated this question for a network that integrates some realistic features. Based on the anatomical data for the rat (DeFelipe, Alonso-Nanclares, & Arellano, 2002), we modeled a portion of the cortex as a layer with periodic boundary conditions respecting the superficial neuron density. This is defined as $\rho_{ve} = \rho_S \sim 28,183$ neurons/mm² with $\rho_V \sim 61,670$ neurons/mm³ for layer 2–3 volume density, and $e \sim 0.457$ mm the depth of these layers. We also took distance-dependent delays with a homogeneous propagation speed of $v_{prop} = 5$ mm/ms. Intrinsic neuron properties are identical to the model used in Vogels and Abbott (2005), and the network contains $N = 10,000$ neurons. Connections for a neuron follow a uniform law on a disc centered on the neuron. We considered as free parameters the radius of the connectivity disc and the proportion of connected neurons p^{conn} inside the disc (see Figure 12f). For a given synaptic strength set $(\Delta g_{exc}, \Delta g_{inh}) = (6, 67)$ nS, we computed the mean excitatory activity as well as the mean interspike interval coefficient of variation to probe the first- and second-order properties of the dynamics (see Figures 12d and 12e). We notice the existence of isostatistics lines where

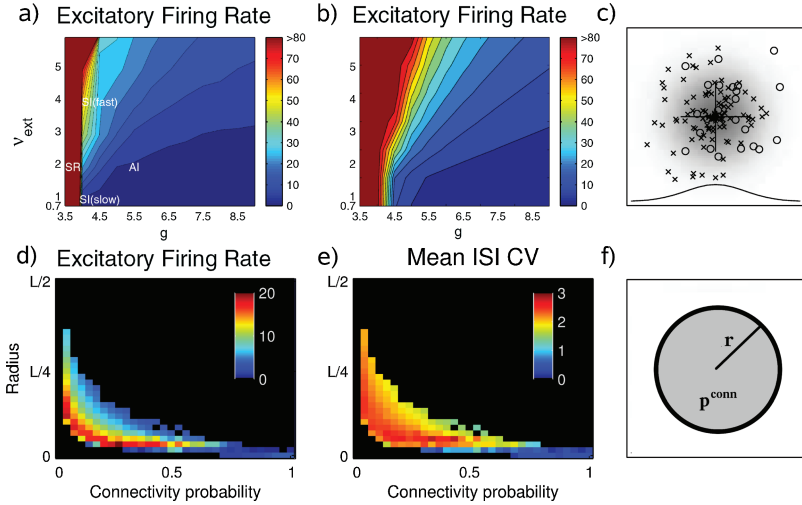


Figure 12: Effect of local network connectivity on macroscopic statistics. (a–c) Comparison of mean excitatory activity for a locally randomly connected current-based network (Mehring et al., 2003) in the (v_{ext}, g) parameter space. (a) Numerical simulations with gaussian distribution (panel reproduced, with permission, from Mehring et al., 2003). (b) First-order mean-field predictions. (c) The gaussian distributed connectivity scheme. (d–f) Effect of local uniformly random connectivity. The parameter space is described by the connectivity disc radius and the connection probability inside the disc. (d) Mean excitatory activity. (e) Mean excitatory interspike interval coefficient of variation. (f) The uniform local random connectivity scheme.

the network displays the same macroscopic behavior. Those lines lie on network configurations where the number of inputs per neuron is constant. Indeed, if the disc radius is increased, the number of incoming synapses will also increase, and it is necessary to decrease the connection probability to recover the same statistical properties. This confirms the previous results shown in Figures 12a and 12b. Interneuron correlations due to more local connections do not seem to invalidate drastically the mean-field predictions as long as the number of connections per neuron is kept fixed and homogeneous. Note that in Figure 12, the case of the randomly connected network does not appear as a stable state because of the distant-dependent delays. Indeed, self-sustained activity cannot occur if the interactions among the network are too slow and we see a large domain of the state diagram that is unstable.

Following the discussion started at the end of the previous section, this result provides an encouraging foundation for large-scale modeling. Indeed, at first sight, it seems intractable to obtain a realistic model of

mesoscopic cortical dynamics when considering the high specificity of the wiring. However, this should not be relevant if population quantities are considered. Extrinsic optical imaging data provide such a quantity that could be related to the master equation variables. Therefore, all high-order patterns in the connectivity should be translated by statistical principles in effective macroscopic coupling available from large-scale data. Further investigations should be devoted to this question to ensure that specific high-order characteristics would not have a dramatic impact on global network dynamics.

4 Discussion

In this letter, we have proposed a mean-field description of AI cortical activity states in balanced networks. We have considered a master equation formalism to describe the activity of networks of size N for timescales larger than a characteristic time T . These numbers were kept finite in order to account for finite-size effects and thus obtain a “mesoscopic” level of description. The resulting phenomenological theory provides a dynamical description of spiking neuron networks that sought to predict state diagrams, but could also be used beyond stability analysis. Furthermore, this framework can be used for any type of neuron as long as its transfer function is known. We obtained a closed set of equations for the mean and variance of the activity and showed that the state diagrams predicted by the mean-field model well matched the diagrams obtained numerically for different types of networks proposed previously (Brunel, 2000; Mehring et al., 2003; Vogels & Abbott, 2005).

Studies of network dynamics have shown that higher-order statistics are crucial in balanced networks. Indeed, chaotic behavior in those systems is produced by the balanced dynamics at the membrane potential level (van Vreeswijk & Sompolinsky, 1996, 1998; Brunel, 2000). Once the mean membrane potential is “clamped” at its subthreshold value, only fluctuations can bring the neuron to fire, thereby providing an irregular firing rate. However, although firing irregularity can be estimated from the stationary interspike interval coefficient of variation (Tuckwell, 1988), no model is able to describe the dynamics of second-order statistics at the network level. The Markovian approach is directly constrained by the population activity correlation’s fine structure during AI states and the minimal bin size to capture network dynamics. According to the numerical model, those values seem to be of the same order, which considerably simplifies the choice of the parameter T .

The master equation model directly relies on the neuron transfer function, which can be chosen according to the desired network model. This transfer function can be exactly determined in current-based networks provided that the input spike trains follow Poisson processes with Dirac synapses (Tuckwell, 1988; Brunel, 2000). However, to cover a broad range of synapse models, we adopt a phenomenological function that can account

for first- and second-order network statistics. For conductance-based models, no exact solution of the equation can be found. We also have to seek approximations to obtain the transfer function. Two main solutions have been proposed: estimating the transfer function numerically (Kumar et al., 2008; Soula & Chow, 2007) or using an approximation with the mean membrane potential of the conductance-based model and the variance taken from an effective current-based model Kuhn et al. (2004). To stay in an analytical framework, we decided to use the second approach, which can easily be implemented in our model.

In current-based models, the predicted state diagrams are in good agreement with the numerical simulations. In this case, the discrepancies are likely to be due to residual correlations caused by finite size effects or by the phenomenological transfer function. Indeed, for activity in small networks that is too low, the diffusion approximation is no longer legitimate, and the corresponding transfer function leads to incorrect predictions. We showed that those frequencies can be better described for larger networks, providing a good model for cortical dynamical regimes. In conductance-based models, the predicted diagrams match the numerical simulations qualitatively but give poor quantitative predictions. It is, however, possible to find an optimized transfer function from a set of functions described by two free parameters. This significantly improves the predictions. In section 3.4.2, we discussed the possibility of adapting this method to dynamics-clamp recordings in order to obtain biophysically more realistic transfer functions directly estimated from real neurons. At a large-scale level, this model could faithfully represent the behavior of conductance-based balanced networks and is therefore a good candidate for building macroscopic models of local field potentials or optical imaging data.

Preliminary results have shown that considering more local connectivities—instead of random schemes—does not alter significantly the master equation predictions as long as the sparseness is strong enough. Therefore, first- and second-order activity statistics do not require an exact description of the network structure. However, heterogeneity among the neurons can be responsible for slight discrepancies between simulations and predictions. Although our model does not take into account specific delays between neurons, for random delays of the order of T , the numerical simulations are even closer to predictions (data not shown). Indeed, global oscillations are destroyed by heterogeneous delays, and the AI region is larger. We are currently working on a systematic study of phase diagrams and their dependence on various parameters.

In conclusion, we have proposed here a mean-field approach to describe the activity of large networks but still staying in the finite-size regime. Such a “mesoscopic” description constitutes a first step toward obtaining a large-scale model of cerebral cortex tissue. The typical size of the networks considered here ($N \sim 5000$ neurons) can be thought of representing the population of cortical neurons seen under one or several pixels of optical

imaging data. Typical values are 100×100 pixels, covering from about 3×3 mm to 3×3 cm of cortical tissue, which gives about 5 to 5000 neurons per pixel in superficial layers according to neuronal densities published previously (Braitenberg & Schüz, 1998). Thus, constructing a 100×100 network of such populations, each described by a master equation analogous to the model presented here, would be possible if the connectivity between adjacent and distant populations could be incorporated in the formalism. This important addition will require studying interconnected networks of neurons in AI states, which constitutes a natural extension of the modeling effort examined in this letter.

Appendix A: Mean Activity and Covariance Matrix Differential Equations

In this appendix, we compute the set of differential equations for the mean activity and the covariance matrix from the master equation. For bin-sized activity defined on the time interval T , the central limit theorem allows one to stop the statistical moment hierarchy at the second order. In other words, we consider a gaussian approximation of the stochastic process. We note the mean activity $\langle m_\mu \rangle$ so that

$$\begin{aligned}
& \partial_t \langle m_\mu \rangle \\
&= \partial_t \prod_{\alpha=1,\dots,K} \int_0^{1/T} dm_\alpha m_\mu P_t(\{m_\gamma\}) \\
&= \prod_{\alpha=1,\dots,K} \int_0^{1/T} dm_\alpha m_\mu \partial_t P_t(\{m_\gamma\}) \\
&= \prod_{\alpha=1,\dots,K} \int_0^{1/T} dm_\alpha \prod_{\beta=1,\dots,K} \int_0^{1/T} dm'_\beta (m_\mu P_t(\{m'_\gamma\}) W(\{m_\gamma\} \mid \{m'_\gamma\})) \\
&\quad - m_\mu P_t(\{m_\gamma\}) W(\{m'_\gamma\} \mid \{m_\gamma\})) \\
&= \prod_{\alpha=1,\dots,K} \int_0^{1/T} dm_\alpha \prod_{\beta=1,\dots,K} \int_0^{1/T} dm'_\beta (m'_\mu - m_\mu) W(\{m'_\gamma\} \mid \{m_\gamma\}) P_t(\{m_\gamma\}) \\
&= \prod_{\alpha=1,\dots,K} \int_0^{1/T} dm_\alpha a_\mu(\{m_\gamma\}) P_t(\{m_\gamma\}) \\
&= \langle a_\mu(\{m_\gamma\}) \rangle,
\end{aligned} \tag{A.1}$$

with

$$a_\mu(\{m_\gamma\}) = \prod_{\beta=1,\dots,K} \int_0^{1/T} dm'_\beta (m'_\mu - m_\mu) W(\{m'_\gamma\} \mid \{m_\gamma\}).$$

To obtain the first-order equation, we develop this function around each populations mean activity values to the second order,

$$\begin{aligned} a_\mu(\{m_\gamma\}) &= a_\mu(\{\langle m_\gamma \rangle\}) + \partial_\lambda a_\mu(\{\langle m_\gamma \rangle\}) \cdot (m_\lambda - \langle m_\lambda \rangle) + \\ &+ \frac{1}{2} \partial_\lambda \partial_\eta a_\mu(\{\langle m_\gamma \rangle\}) \cdot (m_\lambda - \langle m_\lambda \rangle)(m_\eta - \langle m_\eta \rangle) + \mathcal{O}(\delta m^3), \end{aligned}$$

which becomes, after averaging,

$$\langle a_\mu(\{m_\gamma\}) \rangle = a_\mu(\{\langle m_\gamma \rangle\}) + \frac{1}{2} \partial_\lambda \partial_\eta a_\mu(\{\langle m_\gamma \rangle\}) c_{\lambda\eta},$$

where we have introduced the covariance matrix $c_{\lambda\eta} = \langle (m_\lambda - \langle m_\lambda \rangle)(m_\eta - \langle m_\eta \rangle) \rangle$ containing the second-order moments. This gives the first-order set of equations:

$$\begin{aligned} \partial_t \langle m_\mu \rangle &= a_\mu(\{\langle m_\gamma \rangle\}) + \frac{1}{2} \partial_\lambda \partial_\eta a_\mu(\{\langle m_\gamma \rangle\}) c_{\lambda\eta} \\ a_\mu(\{m_\gamma\}) &= \prod_{\alpha=1,\dots,K} \int_0^{1/T} dm'_\alpha (m'_\mu - m_\mu) W(\{m'_\gamma\} \mid \{m_\gamma\}). \end{aligned} \tag{A.2}$$

To compute the second-order equations, we proceed as before:

$$\begin{aligned} \partial_t c_{\mu\nu} &= \partial_t ((m_\mu - \langle m_\mu \rangle)(m_\nu - \langle m_\nu \rangle)) \\ &= \partial_t \langle m_\mu m_\nu \rangle - \partial_t (\langle m_\mu \rangle \langle m_\nu \rangle) \\ &= \partial_t \langle m_\mu m_\nu \rangle - \langle m_\nu \rangle \partial_t \langle m_\mu \rangle - \langle m_\mu \rangle \partial_t \langle m_\nu \rangle. \end{aligned} \tag{A.3}$$

Following the previous equations, we can write,

$$\begin{aligned} \partial_t \langle m_\mu m_\nu \rangle &= \prod_{\alpha=1,\dots,K} \int_0^{1/T} dm'_\alpha \\ &\times \prod_{\beta=1,\dots,K} \int_0^{1/T} dm'_\beta (m'_\mu m'_\nu - m_\mu m_\nu) W(\{m'_\gamma\} \mid \{m_\gamma\}) P_t(\{m_\gamma\}). \end{aligned}$$

Using the relation

$$m'_\mu m'_\nu - m_\mu m_\nu = (m'_\mu - m_\mu)(m'_\nu - m_\nu) + m_\nu(m'_\mu - m_\mu) + m_\mu(m'_\nu - m_\nu),$$

we have

$$\partial_t \langle m_\mu m_\nu \rangle = \langle a_{\mu\nu}(\{m_\gamma\}) \rangle + \langle m_\nu a_\mu(\{m_\gamma\}) \rangle + \langle m_\mu a_\nu(\{m_\gamma\}) \rangle \tag{A.4}$$

with

$$a_{\mu\nu}(\{m_\gamma\}) = \prod_{\beta=1,\dots,K} \int_0^{1/T} dm'_\beta (m'_\beta - m_\mu)(m'_\beta - m_\nu) W(\{m'_\gamma\} \mid \{m_\gamma\}).$$

Inserting equation A.4 into A.3, and using A.1, we get

$$\begin{aligned} \partial_t c_{\mu\nu} &= \langle a_{\mu\nu}(\{m_\gamma\}) \rangle + \langle m_\nu a_\mu(\{m_\gamma\}) \rangle + \langle m_\mu a_\nu(\{m_\gamma\}) \rangle \\ &\quad - \langle m_\nu \rangle \partial_t \langle m_\mu \rangle - \langle m_\mu \rangle \partial_t \langle m_\nu \rangle \\ &= \langle a_{\mu\nu}(\{m_\gamma\}) \rangle + \langle a_\mu(\{m_\gamma\}) \cdot (m_\nu - \langle m_\nu \rangle) \rangle \\ &\quad + \langle a_\nu(\{m_\gamma\}) \cdot (m_\mu - \langle m_\mu \rangle) \rangle. \end{aligned}$$

The first term can be expanded to the second order as we did for the first-order set of equations. Concerning the two other terms, we have,

$$\begin{aligned} &\langle a_\mu(\{m_\gamma\}) \cdot (m_\nu - \langle m_\nu \rangle) \rangle \\ &= \langle (m_\nu - \langle m_\nu \rangle) \cdot (a_\mu(\{m_\gamma\})) \rangle \\ &\quad + \partial_\lambda a_\mu(\{m_\gamma\}) \cdot (m_\lambda - \langle m_\lambda \rangle) + \mathcal{O}(\delta m^3) \\ &= \partial_\lambda a_\mu(\{m_\gamma\}) \langle (m_\nu - \langle m_\nu \rangle)(m_\lambda - \langle m_\lambda \rangle) \rangle + \mathcal{O}(\delta m^3) \\ &= \partial_\lambda a_\mu(\{m_\gamma\}) c_{\nu\lambda} + \mathcal{O}(\delta m^3), \end{aligned}$$

and the same for the third term but with μ and ν inverted. The second-order set of equations can finally be written (van Kampen, 2003)

$$\begin{aligned} \partial_t c_{\mu\nu} &= a_{\mu\nu}(\{m_\gamma\}) + \partial_\lambda a_\mu(\{m_\gamma\}) c_{\nu\lambda} + \partial_\lambda a_\nu(\{m_\gamma\}) c_{\mu\lambda} \\ a_{\mu\nu}(\{m_\gamma\}) &= \prod_{\alpha=1,\dots,K} \int_0^{1/T} dm'_\alpha (m'_\alpha - m_\mu)(m'_\alpha - m_\nu) W(\{m'_\gamma\} \mid \{m_\gamma\}). \end{aligned} \tag{A.5}$$

Appendix B: Correlation Matrix Differential Equation

In this appendix, we compute the set of differential equations that describes the correlation matrix in a stationary state. The derivation is slightly different from the computation in appendix A. A similar computation has been done in Ginzburg and Sompolinsky (1994). The derivative can be written as:

$$\begin{aligned} \partial_\tau \text{Corr}_{\mu\nu}(\tau) &= \partial_\tau (\langle m_\mu(t) - \langle m_\mu(t) \rangle \rangle (m_\nu(t+\tau) - \langle m_\nu(t+\tau) \rangle)) \\ &= \partial_\tau (\langle m_\mu(t)m_\nu(t+\tau) \rangle - \langle m_\mu(t) \rangle \langle m_\nu(t+\tau) \rangle). \end{aligned} \tag{B.1}$$

If we consider the first term of equation B.1,

$$\begin{aligned}
& \partial_\tau \langle m_\mu(t) m_\nu(t + \tau) \rangle = \\
&= \partial_\tau \prod_{\alpha=1,\dots,K} \int_0^{1/T} dm_\alpha \prod_{\beta=1,\dots,K} \int_0^{1/T} dm'_\beta m_\mu m'_\nu P(\{m'_\gamma\}, t \\
&\quad + \tau | \{m_\gamma\}, t) P_t(\{m_\gamma\}) \\
&= \prod_{\alpha=1,\dots,K} \int_0^{1/T} dm_\alpha m_\mu \left(\prod_{\beta=1,\dots,K} \int_0^{1/T} dm'_\beta m'_\nu \partial_\tau P(\{m'_\gamma\}, t \right. \\
&\quad \left. + \tau | \{m_\gamma\}, t \right) P_t(\{m_\gamma\}).
\end{aligned}$$

The conditional probability $P(\{m'_\gamma\}, t + \tau | \{m_\gamma\}, t)$ is also a solution of the master equation, so that the term in the bracket is similar to equation A.1, and we can write

$$\partial_\tau \langle m_\mu(t) m_\nu(t + \tau) \rangle = \langle m_\mu(t) a_\nu(\{m_\gamma(t + \tau)\}) \rangle. \quad (\text{B.2})$$

The second term in equation A.1 is simply

$$\begin{aligned}
\partial_\tau \langle m_\mu(t) \rangle \langle m_\nu(t + \tau) \rangle &= \partial_\tau \langle m_\mu(t) \rangle \partial_\tau \langle m_\nu(t + \tau) \rangle \\
&= \langle m_\mu(t) \rangle \langle a_\nu(\{m_\gamma(t + \tau)\}) \rangle.
\end{aligned} \quad (\text{B.3})$$

Combining equations B.2 and B.3 into B.1, we get

$$\partial_\tau \text{Corr}_{\mu\nu}(\tau) = \langle (m_\mu(t) - \langle m_\mu(t) \rangle) a_\nu(\{m_\gamma(t + \tau)\}) \rangle. \quad (\text{B.4})$$

As we are considering time-scales that are beyond the decreasing time of the network activity correlations, we can develop $a_\nu(\{m_\gamma(t + \tau)\})$ around the mean values to the second order,

$$\begin{aligned}
a_\nu(\{m_\gamma(t + \tau)\}) &= a_\nu(\{\langle m_\gamma(t + \tau) \rangle\}) + \partial_\lambda a_\nu(\{\langle m_\gamma(t + \tau) \rangle\}) \\
&\quad \times (m_\lambda(t + \tau) - \langle m_\lambda(t + \tau) \rangle) + \mathcal{O}(\delta m^2),
\end{aligned}$$

so that equation B.4 becomes, to second order,

$$\partial_\tau \text{Corr}_{\mu\nu}(\tau) = \partial_\lambda a_\nu(\{\langle m_\gamma(t + \tau) \rangle\}) \text{Corr}_{\mu\lambda}(\tau). \quad (\text{B.5})$$

We are interested in the activity correlations in the stationary state; therefore, the mean activities $\{\langle m_\gamma \rangle\}$ no longer depend on τ . Moreover, the initial

conditions for those differential equations are given by the stationary values of the covariance matrix.

Appendix C: Conductance-Based Synaptic Functions for the Master Equation

In this appendix, we compute the remaining functions necessary to use the conductance-based model. The effective time constant is activity dependent in the conductance-based model, and it is given by

$$\langle \tau_{\mu}^{eff} \rangle = \frac{1}{\frac{1}{\tau_{\mu}^{mem}} + \sum_{\alpha=1,\dots,K} \frac{\langle G_{\alpha\mu} \rangle}{C_{\mu}}}.$$

We need to compute the first and second derivatives:

$$\begin{aligned}\partial_{\lambda} \langle \tau_{\mu}^{eff} \rangle &= -\langle \tau_{\mu}^{eff} \rangle^2 \frac{\Phi_{\lambda\mu}}{E_{\lambda}} \\ \partial_{\eta} \partial_{\lambda} \langle \tau_{\mu}^{eff} \rangle &= 2 \langle \tau_{\mu}^{eff} \rangle^3 \frac{\Phi_{\eta\mu}}{E_{\eta}} \frac{\Phi_{\lambda\mu}}{E_{\lambda}}.\end{aligned}$$

The function $\Psi_{\alpha\mu}$ depends on the chosen synapse, and we compute the corresponding derivatives for exponential and α -synapses:

- Exponential synapses. The function is given by

$$\Psi_{\alpha\mu}^{Exp} = \frac{C_{\alpha\mu}}{\tau_{\alpha} + \langle \tau_{\mu}^{eff} \rangle} \left(\frac{\tau_{\alpha} \Delta g_{\alpha\mu} \langle \tau_{\mu}^{eff} \rangle (E_{\alpha} - \langle V_{\mu} \rangle)}{C_{\mu}} \right)^2,$$

so that

$$\begin{aligned}\partial_{\lambda} \Psi_{\alpha\mu}^{Exp} &= \Psi_{\alpha\mu}^{Exp} \left(\partial_{\lambda} \langle \tau_{\mu}^{eff} \rangle \left(\frac{2}{\langle \tau_{\mu}^{eff} \rangle} - \frac{1}{\langle \tau_{\mu}^{eff} \rangle + \tau_{\alpha}} \right) \right. \\ &\quad \left. - \frac{2 \partial_{\lambda} Q_{\mu}}{(E_{\alpha} - \langle V_{\mu} \rangle)} \right) \\ \partial_{\eta} \partial_{\lambda} \Psi_{\alpha\mu}^{Exp} &= \frac{\partial_{\eta} \Psi_{\alpha\mu} \partial_{\lambda} \Psi_{\alpha\mu}}{\Psi_{\alpha\mu}} + \Psi_{\alpha\mu} \left(\partial_{\eta} \partial_{\lambda} \langle \tau_{\mu}^{eff} \rangle \right. \\ &\quad \times \left(\frac{2}{\langle \tau_{\mu}^{eff} \rangle} - \frac{1}{\langle \tau_{\mu}^{eff} \rangle + \tau_{\alpha}} \right) + \partial_{\eta} \langle \tau_{\mu}^{eff} \rangle \partial_{\lambda} \langle \tau_{\mu}^{eff} \rangle \right. \\ &\quad \times \left(\frac{1}{(\langle \tau_{\mu}^{eff} \rangle + \tau_{\alpha})^2} - \frac{2}{\langle \tau_{\mu}^{eff} \rangle^2} \right) \\ &\quad \left. - \frac{2 \partial_{\lambda} Q_{\mu} \partial_{\eta} Q_{\mu}}{(E_{\alpha} - \langle V_{\mu} \rangle)} - \frac{2 \partial_{\lambda} \partial_{\eta} Q_{\mu}}{(E_{\alpha} - \langle V_{\mu} \rangle)^2} \right).\end{aligned}$$

- α -synapses. Similarly

$$\begin{aligned}\Psi_{\alpha\mu}^{\alpha syn} = & \frac{1}{2} C_{\alpha\mu} (2\langle\tau_{\mu}^{eff}\rangle + \tau_{\alpha}) \\ & \times \left(\frac{e\tau_{\alpha}\Delta g_{\alpha\mu}\langle\tau_{\mu}^{eff}\rangle(E_{\alpha} - \langle V_{\mu}\rangle)}{C_{\mu}(\tau_{\alpha} + \langle\tau_{\mu}^{eff}\rangle)} \right)^2,\end{aligned}$$

so that

$$\begin{aligned}\partial_{\lambda}\Psi_{\gamma\mu} = & 2\Psi_{\gamma\mu} \left(\partial_{\lambda}\langle\tau_{\mu}^{eff}\rangle \left(\frac{1}{(2\langle\tau_{\mu}^{eff}\rangle + \tau_{\gamma})} + \frac{1}{\langle\tau_{\mu}^{eff}\rangle} \right. \right. \\ & \left. \left. - \frac{1}{(\langle\tau_{\mu}^{eff}\rangle + \tau_{\gamma})} \right) - \frac{\partial_{\lambda}Q_{\mu}}{(E_{\gamma} - \langle V_{\mu}\rangle)} \right) \\ \partial_{\eta}\partial_{\lambda}\Psi_{\gamma\mu} = & \frac{\partial_{\lambda}\Psi_{\gamma\mu}\partial_{\eta}\Psi_{\gamma\mu}}{\Psi_{\gamma\mu}} \\ & + \left(\partial_{\eta}\partial_{\lambda}\langle\tau_{\mu}^{eff}\rangle \left(\frac{1}{(2\langle\tau_{\mu}^{eff}\rangle + \tau_{\gamma})} + \frac{1}{\langle\tau_{\mu}^{eff}\rangle} \right. \right. \\ & \left. \left. - \frac{1}{(\langle\tau_{\mu}^{eff}\rangle + \tau_{\gamma})} \right) \right. \\ & \left. + \partial_{\eta}\langle\tau_{\mu}^{eff}\rangle\partial_{\lambda}\langle\tau_{\mu}^{eff}\rangle \left(\frac{1}{((\langle\tau_{\mu}^{eff}\rangle + \tau_{\gamma})^2} \right. \right. \\ & \left. \left. - \frac{2}{(2\langle\tau_{\mu}^{eff}\rangle + \tau_{\gamma})^2} - \frac{1}{\langle\tau_{\mu}^{eff}\rangle^2} \right) \right. \\ & \left. - \frac{\partial_{\eta}\partial_{\lambda}Q_{\mu}}{(E_{\gamma} - \langle V_{\mu}\rangle)} - \frac{\partial_{\eta}Q_{\eta}\partial_{\lambda}Q_{\mu}}{(E_{\gamma} - \langle V_{\mu}\rangle)^2} \right).\end{aligned}$$

Acknowledgments

The research was supported by the CNRS, ANR, and the European Community (FACETS grant FP6 15879). We thank Olivier Marre, Pierre Yger, Nicolas Brunel, and Romain Brette for fruitful discussions and comments on the manuscript.

References

- Amit, D. J., & Brunel, N. (1997). Model of global spontaneous activity and local structured activity during delay periods in the cerebral cortex. *Cereb. Cortex*, 7, 237–252.
- Braitenberg, V., & Schüz, A. (1998). *Cortex: Statistics and geometry of neuronal connectivity* (2nd ed.). Berlin: Springer-Verlag.
- Brette, R., Rudolph, M., Carnevale, T., Hines, M., Beeman, D., Bower, J. M., et al. (2007). Simulation of networks of spiking neurons: A review of tools and strategies. *J. Comput. Neurosci.*, 23, 349–398.
- Brunel, N. (2000). Dynamics of sparsely connected networks of excitatory and inhibitory spiking neurons. *J. Comput. Neurosci.*, 8, 183–208.
- Brunel, N., & Hakim, V. (1999). Fast global oscillations in networks of integrate-and-fire neurons with low firing rates. *Neural Comput.*, 11, 1621–1671.
- Brunel, N., & Sergi, S. (1998). Firing frequency of leaky integrate-and-fire neurons with synaptic currents dynamics. *J. Theor. Biol.*, 195, 87–95.
- Crutchfield, J. P., & Kaneko, K. (1988). Are attractors relevant to turbulence? *Phys. Rev. Lett.*, 60, 2715–2718.
- DeFelipe, J., Alonso-Nanclares, L., & Arellano, J.I. (2002). Microstructure of the neocortex: Comparative aspects. *J. Neurocytology*, 39, 299–316.
- Destexhe, A., & Contreras, D. (2006). Neuronal computations with stochastic network states. *Science*, 314, 85–90.
- Destexhe, A., Rudolph, M., & Paré, D. (2003). The high-conductance state of neocortical neurons in vivo. *Nature Reviews Neurosci.*, 4, 739–751.
- El Boustani, S. (2006). *Information transport in networks during irregular activity states* (in French). Master's thesis, Ecole Normale Supérieure, France.
- El Boustani, S., & Destexhe, A. (2007). Mesoscopic model of balanced neuron networks using a master equation formalism. (abstract) In *Computation and Neural Systems 2007 Conference*. Available online at <http://www.cnsorg.org>.
- El Boustani, S., Pospischil, M., Rudolph-Lilith, M., & Destexhe, A. (2007). Activated cortical states: Experiments, analyses and models. *J. Physiol. Paris* 101, 99–109.
- Fourcaud, N., & Brunel, N. (2002). Dynamics of the firing probability of noisy integrate-and-fire neurons. *Neural Comput.*, 14, 2057–2110.
- Gerstner, W. (2000). Population dynamics of spiking neurons: Fast transients, asynchronous states, and locking. *Neural Comput.*, 12, 43–89.
- Ginzburg, I., & Sompolinsky, H. (1994). Theory of correlations in stochastic neural networks. *Phys. Rev.*, 50, 3171–3191.
- Hertz, J., Lechner, A., & Ahmadi, M. (2004). Mean field methods for cortical network dynamics. *Comput. Neurosci.*, 3146, 71–89.
- Kuhn, A., Aertsen, A., & Rotter, S. (2004). Neuronal integration of synaptic input in the fluctuation-driven regime. *J. Neurosci.*, 24, 2345–2356.
- Kumar, A., Schrader, S., Aertsen, A., & Rotter, S. (2008). The high-conductance state of cortical networks. *Comput. Neurosci.*, 20, 1–43.
- Latham, P. E., Richmond, B. J., Nelson, P. G., & Nirenberg, S. (2000). Intrinsic dynamics in neuronal networks. I. Theory. *J. Neurophysiol.*, 83, 808–827.

- Matsumura, M., Cope, T., & Fetz, E. E. (1988). Sustained excitatory synaptic input to motor cortex neurons in awake animals revealed by intracellular recording of membrane potentials. *Exp. Brain Res.*, 70, 463–469.
- Mehring, C., Hehl, U., Kubo, M., Diesmann, M., & Aertsen, A. (2003). Activity dynamics and propagation of synchronous spiking in locally connected random networks. *Biol. Cybern.*, 88, 395–408.
- Ohira, T., & Cowan, J. D. (1993). Master-equation approach to stochastic neurodynamics. *Phys. Rev. E*, 48, 2259–2266.
- Plesser, H. E., & Gerstner, W. (2000). Noise in integrate-and-fire neurons: From stochastic input to escape rates. *Neural Comput.*, 12, 367–384.
- Soula, H., & Chow, C. C. (2007). Stochastic dynamics of a finite-size spiking neural network. *Neural Comput.*, 19, 3262–3292.
- Steriade, M., Timofeev, I., & Grenier, F. (2001). Natural waking and sleep states: A view from inside neocortical neurons. *J. Neurophysiol.*, 85, 1969–1985.
- Tuckwell, H. C. (1988). *Introduction to theoretical neurobiology*. Cambridge: Cambridge University Press.
- van Kampen, N. G. (2003). *Stochastic processes in physics and chemistry*. Amsterdam: North-Holland Personal Library.
- van Vreeswijk, C., & Sompolinsky, H. (1996). Chaos in neuronal networks with balanced excitatory and inhibitory activity. *Science*, 274, 1724–1726.
- van Vreeswijk, C., & Sompolinsky, H. (1998). Chaotic balanced state in a model of cortical circuits. *Neural Comput.*, 10, 1321–1371.
- Vogels, T. P., & Abbott, L. F. (2005). Signal propagation and logic gating in networks of integrate-and-fire neurons. *J. Neurosci.*, 25, 10786–10795.

Received February 12, 2008; accepted May 16, 2008.